

BRANCHED SIGNATURE KERNEL SOLVERS FOR ODES WITH ROUGH SINGLE-TRAJECTORY SIGNALS

MUNAWAR ALI* QI FENG† CHARLIE PYLE‡ GEORGE XU##

ABSTRACT. We develop a branched signature kernel solver for linear and nonlinear ordinary differential equations driven by a *single observed trajectory* of a possibly rough forcing signal — a setting that arises naturally in earthquake engineering, finance, biology, and structural health monitoring, where the forcing is observed exactly once and the solver must respect the underlying physical law without recourse to an ensemble of realizations. Two ingredients are new. First, a *count-sampling* construction turns the single observation into a hierarchical family of $N + 1$ nested training paths on which the branched signature kernel can be evaluated; this allows the signature kernel machinery, originally designed for multi-realization regression problems, to operate on a single-trajectory observation. Second, a kernel-collocation framework places the ansatz either on the highest-order derivative of the solution (with lower derivatives recovered by integrating the kernel) or on the solution itself (after m -fold integration of the ODE). We prove a universal approximation theorem for the branched signature kernel, leveraging the Hairer–Kelly morphism to express branched signature evaluations through geometric signatures of time-extended paths. The offline solver is extended to a streaming Test/Train/Retrain protocol with closed-form online updates in the linear case and scalar Newton steps in the nonlinear case. Numerical experiments on six benchmarks (El-Centro earthquake displacement, the Solow capital-stock model, an fBM-driven second-order ODE, a forced Duffing oscillator, a path-dependent Arias-intensity-degraded oscillator with variable coefficients, and a noisy Kuramoto phase-oscillator system) show that the branched signature-kernel solver delivers accurate, stable predictions across all regimes.

Keywords: Branched Signature; Branched Signature Kernel; Universal approximation theorem; fractional Brownian motion; Hopf algebra; ODE solver; count sampling; streaming kernel methods.
2000 AMS Mathematics subject classification: 60L10, 60L20, 46E22, 60G17, 65C20, 65C30, 60H10, 91B70.

1. INTRODUCTION

The numerical solution of ordinary differential equations driven by a *single observed forcing trajectory* arises in many engineering and scientific settings. A structure responding to a recorded ground acceleration during an earthquake, a financial state variable evolving under a single realized market signal, a biological process excited by a particular environmental input, and a coupled oscillator network perturbed by one realization of noise are all instances of the same mathematical problem: solve $\mathcal{N}\mathbf{u}(t) = f(t)$ on $[0, T]$ given a single discrete sample of f . Two features distinguish this regime from the classical setting of numerical analysis. First, no ensemble of independent realizations of f is available; ensemble-averaged calibration is therefore impossible. Second, the observed forcing is typically rough — high-frequency seismic accelerations, fractional Brownian volatility, and noisy

Date: May 26, 2026.

*: Department of Mathematics, Florida State University, Tallahassee, FL 32306; e-mail: ma22bm@fsu.edu.

†: Department of Mathematics, Florida State University, Tallahassee, FL 32306; e-mail: qfeng2@fsu.edu. This author is partially supported by the National Science Foundation under grant #DMS-2420029.

‡: Department of Mathematics, Texas A&M University, College Station, TX 77843; e-mail: charliepyle@tamu.edu. This author is partially supported by the National Science Foundation under grant #DMS-2420029 through the Research Experience for Undergraduates (REU) program at Florida State University.

##: Department of Mathematics, Rutgers University, Piscataway, NJ 08854; e-mail: gtx1@scarletmail.rutgers.edu. This author is partially supported by the National Science Foundation under grant #DMS-2420029 through the Research Experience for Undergraduates (REU) program at Florida State University.

biological signals all exhibit Hölder regularity well below the bounded-variation assumption underlying classical numerical-analysis theory. A solver that respects the physical law governing the ODE while learning a representation of the solution from a single rough trajectory is therefore needed.

In the literature, signatures have been successful in encoding path information. In particular, signatures of geometric rough paths [Lyons et al., 2007, Friz and Victoir, 2010] and branched signatures for branched rough paths [Gubinelli, 2010] have been developed as fundamental objects in rough path theory. Uniqueness results of increasing generality were established in [Hambly and Lyons, 2010, Boedihardjo et al., 2016, Cuchiero et al., 2023], and universal approximation theorems for continuous functions on path space were proved in [Lyons, 2014, Chevyrev and Oberhauser, 2022, Cuchiero et al., 2023, Chevyrev and Kormilitzin, 2025, Cuchiero et al., 2025, Cox et al., 2026, Ceylan et al., 2026]. Pairing two signatures via an inner product yields the *signature kernel*, introduced by [Király and Oberhauser, 2019], who lifted static kernels to path space via the signature transform; [Salvi et al., 2021] characterized the signature kernel as the solution of a Goursat partial differential equation, enabling its efficient computation, and [Toth et al., 2024] developed random Fourier signature features for scalable kernel evaluation. The branched signature model of [Ali and Feng, 2025] provides the rough-path foundation for our branched signature kernel construction; the distinction is that [Ali and Feng, 2025] works at the feature-vector level, whereas we work at the reproducing-kernel level, which permits both the universal approximation theorem and the single-trajectory collocation solver developed in this paper.

It is often useful to consider different lifts or augmentations of paths before taking the signature transform, in order to capture features or underlying information within streams of data. Time augmentation, basepoint augmentation, and lead-lag augmentation are discussed in [Chevyrev and Kormilitzin, 2025, Lyons and McLeod, 2025, Chevyrev and Oberhauser, 2022, Király and Oberhauser, 2019]; time augmentation in particular guarantees signature uniqueness and universal approximation [Király and Oberhauser, 2019, Chevyrev and Oberhauser, 2022], while lead-lag augmentation, popularized by [Gyurkó et al., 2013, Lyons and McLeod, 2025, Chevyrev and Kormilitzin, 2025], captures quadratic variation and is used heavily in financial applications. [Kidger et al., 2019] introduced the learned augmentation in which a neural network learns the transformation that precedes the signature, leading to the Signatory library. In this paper we view path augmentation as a transformation that lifts a branched rough path into a geometric rough path; taking the signature kernel of the augmented path then yields the branched signature kernel of the original path. We further introduce an RBF lift of the signature that empirically improves performance in our numerical experiments. On the computational side, efficient raw signature implementations are available in `iisignature` [Reizenstein and Graham, 2020], `Signatory` [Kidger and Lyons, 2021], `PySigLib` [Shmelev and Salvi, 2025], and `KerasSig` [Genet and Inzirillo, 2025], with Chen’s identity [Chevyrev and Kormilitzin, 2025] enabling reuse of sub-path signatures through the “stream” features of `Signatory` and `KerasSig`. For signature kernels specifically, `KSig` [Tóth et al., 2025] provides GPU-accelerated dynamic-programming, low-rank, random-Fourier, and PDE-based implementations, and `PySigLib` offers PyTorch-compatible kernel computations with backpropagation support. Our count-sampling construction is particularly compatible with these libraries: the nested training paths share prefix signatures, allowing the entire family $\{f_0, \dots, f_N\}$ to be processed at essentially the cost of the longest path.

Signature-based models have found use across finance, medicine, and signal processing [Lemerrier et al., 2021, Lyons, 2014, Levin et al., 2016, Zeng and Jiang, 2025, Bayer et al., 2025, Chevyrev and Kormilitzin, 2025]. In finance, signatures’ affinity for rough volatility makes them a natural tool for option pricing, nowcasting, and optimal stopping [Gyurkó et al., 2013, Mohaddes et al., 2025, Alòs et al., 2025, Cohen et al., 2023, Horvath et al., 2023, Lyons et al., 2020]. For differential equations, the closest precedent to our solver is the signature-kernel path-dependent PDE solver of [Pannier and Salvi, 2024], which fits an RKHS minimum-norm interpolant of the PPDE solution at a set of collocation points; that solver,

however, requires *multiple* realizations of the driving path and does not employ branched signatures. Our framework removes both restrictions: a single trajectory suffices via count-sampling, and the branched signature kernel resolves the higher-order brackets that distinguish branched roughness from geometric roughness. Neural-network signature solvers for path-dependent PDEs have been proposed in [Feng et al., 2023, Sabate-Vidales et al., 2020, Fang et al., 2023, Bayraktar et al., 2024] and extended to kernel frameworks in [Issa et al., 2023]; both lines likewise rely on multiple path realizations. The classical kernel-collocation methodology underlying our solver traces back to the Kansa method [Kansa, 1990b, Kansa, 1990a] for RBF-based PDE solving, with subsequent developments in RBF and RKHS methods for differential equations [Fornberg and Flyer, 2015, Abbasbandy et al., 2015] and in Gaussian-process priors for nonlinear PDE solvers [Chen et al., 2021], the latter informing our choice of regularization and warm-starting strategies in the nonlinear case. Finally, the Test/Train/Retrain protocol developed in this paper is a kernel-method analogue of the online-updating literature — we exploit the block structure of the augmented kernel matrix to update only the newest block in closed form, with periodic full-batch retraining on a sliding window to control drift — and parallels, in spirit, the recursive least-squares and online kernel-ridge-regression traditions, but to our knowledge has not previously been instantiated for signature kernel solvers of ODEs.

Based on the above ideas, we develop a branched signature kernel collocation solver that operates on a *single observed forcing trajectory* — the central novelty of this paper. At the heart of the construction is a *count-sampling* scheme that turns one discrete observation of the forcing into a hierarchical family of nested training paths $\mathbf{f}_0 \subset \mathbf{f}_1 \subset \dots \subset \mathbf{f}_N$, on which the branched signature kernel is natively evaluated and across which Chen’s identity yields prefix-sharing speedups; to our knowledge this single-trajectory training set is new in the literature. Building on it, we develop two complementary collocation formulations — a differential ansatz on the highest-order derivative $\mathbf{u}^{(m)}$ and an integral ansatz on \mathbf{u} itself (preferable for rough forcings, since the ODE is integrated m times before fitting) — both applicable to multidimensional linear and nonlinear systems. We prove a universal approximation theorem for the branched signature kernel, which establishes the model as a universal hypothesis class for continuous functionals of the forcing path. Numerically, the branched signature kernel is computed via the Hairer–Kelly morphism [Hairer and Kelly, 2015], whose approximation by a neural network was first proposed in [Ali and Feng, 2025]. The offline solver is then extended to a streaming Test/Train/Retrain protocol with closed-form $O(nd^2 + d^3)$ online updates in the linear case and scalar Newton steps in the nonlinear case.

The paper is organized as follows. In Section 2, we introduce the basic concepts of signatures and signature kernels. In Section 3, we introduce the branched signature kernel model and prove a universal approximation theorem for this model. In Section 4, we develop branched signature kernel solvers for linear ODE systems, including the *linear integral method* and its m -fold-integrated variant, as well as for nonlinear ODE systems via the *nonlinear integral method*. In Section 5, we extend the offline solver to a streaming protocol with closed-form online updates in the linear case and scalar Newton updates in the nonlinear case, and present a periodic retraining algorithm. In Section 6, we present numerical experiments on the El-Centro earthquake displacement model, the Solow capital-stock model, a fractional-Brownian-motion-driven linear ODE, the forced Duffing oscillator, a variable coefficient path-dependent Arias intensity degraded single degree of freedom (SDOF) equation, and the rough Kuramoto phase oscillator system, with side-by-side comparisons of the branched and non-branched constructions across all benchmarks.

2. PRELIMINARIES

In this section, we first provide a self-contained introduction to signatures and signature kernels. We then define the branched signature [Ali and Feng, 2025] and the corresponding branched signature kernels.

To begin with, we will set some terminology that will help us to talk about signatures and signature kernels.

Definition 2.1 (Path). A path \mathbf{X} from some time interval $[0, T]$ to \mathcal{H} is a continuous mapping written as

$$\mathbf{X} : [0, T] \rightarrow \mathcal{H}.$$

Also, we define $\mathbf{X}_{s,t} = \mathbf{X}_t - \mathbf{X}_s$ as an increment of the path.

Unless otherwise stated, we will be working with the paths that take values in the finite dimensional Hilbert space \mathcal{H} with $\dim(\mathcal{H}) = d$. Let \mathcal{A} be the alphabet set corresponding to \mathcal{H} given as $\mathcal{A} = \{1, 2, \dots, d\}$. We define a word \mathbf{w} of length $|\mathbf{w}| = k$ to be sequence $\mathbf{w} = w_1 \cdots w_k$, where $w_i \in \mathcal{A}$ for $i = 1, 2, \dots, k$. Let \mathbf{W} be the set of all words made from the alphabet \mathcal{A} . Define

$$\mathbf{W}_n := \begin{cases} \{\mathbf{w} = w_1 \cdots w_k : |\mathbf{w}| = n\}, & n \neq 0, \\ \emptyset, & n = 0. \end{cases}$$

Definition 2.2 (Concatenation of words). For two words $\mathbf{v} = v_1 \cdots v_j$ and $\mathbf{w} = w_1 \cdots w_k$, we define their concatenation \mathbf{vw} as

$$\mathbf{vw} = v_1 \cdots v_j w_1 \cdots w_k.$$

The signature of a path defined on \mathcal{H} lives in the space called **extended tensor algebra** over \mathcal{H} defined as

$$T((\mathcal{H})) = \prod_{n=0}^{\infty} (\mathcal{H})^{\otimes n} = \{\mathbf{v} = (v_0, v_1, \dots, v_n, \dots) \mid v_n \in (\mathcal{H})^{\otimes n}, n = 0, 1, \dots\},$$

where $(\mathcal{H})^{\otimes 0} := \mathbb{R}$. We also define the **tensor algebra** over \mathcal{H} to be the space $T(\mathcal{H})$ defined by

$$T(\mathcal{H}) = \bigoplus_{n=0}^{\infty} (\mathcal{H})^{\otimes n} = \{\mathbf{v} \in T((\mathcal{H})) \mid \forall \mathbf{v} \exists K \in \mathbb{N} \text{ such that } v_n = 0 \forall n \geq K\},$$

where most of the components of the infinite dimensional object $\mathbf{v} \in T((\mathcal{H}))$ are zero. If we want to restrict the non-zero components then we have the **truncated tensor algebra** over \mathcal{H} which is defined as

$$T^N(\mathcal{H}) := \{\mathbf{v} \in T(\mathcal{H}) \mid v_n = 0 \forall n > N\}.$$

Next, define paths of bounded p -variation for $p = 1$ also called paths of bounded variation.

Definition 2.3 (Paths of bounded variation). Let \mathcal{H} be a Hilbert space. We denote the set of \mathcal{H} -valued paths of bounded variation on $[0, 1]$ starting at the origin by

$$C^1([0, 1], \mathcal{H}) := \{\mathbf{X} \in C([0, 1], \mathcal{H}) : \mathbf{X}(0) = 0, \|\mathbf{X}\|_1 < \infty\}$$

where $\|\mathbf{X}\|_1 = \sup_{\pi} \sum_{i=1}^{l-1} \|\mathbf{X}(t_{i+1}) - \mathbf{X}(t_i)\|_{\mathcal{H}}$ and the supremum is taken over all finite partitions $\pi = \{(t_i)_{i=1, \dots, l} : 0 = t_1 < \dots < t_l = 1\}$ of $[0, 1]$.

Though we will be working with paths of bounded p -variation for any $p \geq 1$, the signature of bounded p -variation for $p = 1$ is canonically defined using Riemann–Stieltjes integration.

Definition 2.4 (Signature of path). The signature of an \mathcal{H} -valued path $(\mathbf{X}_t)_{t \in [0, T]}$ is an infinite dimensional object $\mathbf{Sig}(\mathbf{X})_{st}$ that belongs to the space $T((\mathcal{H}))$ and is defined as

$$\mathbf{Sig}(\mathbf{X})_{st} = \left(1, \int_s^t d\mathbf{X}_r^{w_i}, \int_s^t \int_s^{r_2} d\mathbf{X}_{r_1}^{w_i} d\mathbf{X}_{r_2}^{w_j}, \int_s^t \int_s^{r_3} \int_s^{r_2} d\mathbf{X}_{r_1}^{w_i} d\mathbf{X}_{r_2}^{w_j} d\mathbf{X}_{r_3}^{w_k}, \dots \right)_{w_i, w_j, w_k, \dots \in \mathcal{A}}.$$

Equivalently, the signature of a continuous \mathcal{H} -valued path of bounded variation $(\mathbf{X}_t)_{t \in [0, T]}$ is a $T((\mathcal{H}))$ -valued process $(s, t) \in \Delta_T^2 \mapsto \mathbf{Sig}(\mathbf{X})_{st} \in T((\mathcal{H}))$ also defined recursively as follows

$$\langle \mathbf{Sig}(\mathbf{X})_{st}, \emptyset \rangle := 1, \quad \langle \mathbf{Sig}(\mathbf{X})_{st}, \mathbf{w} \rangle := \int_s^t \langle \mathbf{Sig}(\mathbf{X})_{sr}, w_1 \cdots w_{n-1} \rangle d\mathbf{X}_r^{w_n},$$

for each word $\mathbf{w} = w_1 \dots w_n \in \mathbf{W}$ and $\Delta_T^2 := \{(s, t) \in [0, T]^2 : 0 \leq s \leq t \leq T\}$.

The signature of a path of bounded variation enjoys many nice properties. Some of them are shuffle product and the Chen's identity. To talk about shuffle product of signature components, let us define shuffle product of words \mathbf{w} in \mathbf{W} first.

Definition 2.5 (Shuffle Product). Let \emptyset denote the empty word. For words \mathbf{u}, \mathbf{v} and letters a, b , the shuffle product is defined recursively by

$$\mathbf{u} \sqcup \emptyset = \emptyset \sqcup \mathbf{u} = \mathbf{u},$$

and

$$(\mathbf{u}a) \sqcup (\mathbf{v}b) = (\mathbf{u} \sqcup \mathbf{v}b)a + (\mathbf{u}a \sqcup \mathbf{v})b.$$

If we fix a basis $\{e_1, \dots, e_d\}$ of \mathcal{H} , and for a word $\mathbf{w} = w_1 \dots w_n$, define $e_{\mathbf{w}} := e_{w_1} \otimes \dots \otimes e_{w_n}$, $e_{\emptyset} := 1$, then the shuffle product extends from words to elements of $T(\mathcal{H})$ by

$$\mathbf{x} \sqcup \mathbf{y} = \sum_{\mathbf{u}, \mathbf{v}} x_{\mathbf{u}} y_{\mathbf{v}} (e_{\mathbf{u}} \sqcup e_{\mathbf{v}}),$$

where $\mathbf{x} = \sum_{\mathbf{u}} x_{\mathbf{u}} e_{\mathbf{u}}, \mathbf{y} = \sum_{\mathbf{u}} y_{\mathbf{u}} e_{\mathbf{u}} \in T(\mathcal{H})$. Following this definition, if we endow the space $T(\mathcal{H})$ with the shuffle product \sqcup then the quadruple $(T(\mathcal{H}), +, \cdot, \sqcup)$ is an associative algebra.

Definition 2.6 (Shuffle Property). [Lyons et al., 2007] Let $(\mathbf{X}_t)_{t \in [0, T]}$ be a continuous \mathcal{H} -valued path of bounded variation and $\mathbf{u} = u_1 \dots u_n$ and $\mathbf{v} = v_1 \dots v_m$ be two words, then

$$\langle \mathbf{Sig}(\mathbf{X})_{st}, \mathbf{u} \rangle \langle \mathbf{Sig}(\mathbf{X})_{st}, \mathbf{v} \rangle = \langle \mathbf{Sig}(\mathbf{X})_{st}, \mathbf{u} \sqcup \mathbf{v} \rangle.$$

Remark 2.7. The shuffle property reduces to the classical integration by parts identity when $|\mathbf{u}| = 1$ and $|\mathbf{v}| = 1$.

The signature of a path also enjoys another nice property called Chen's identity that is stated in the following proposition.

Proposition 2.8 (Chen's Identity). [Friz and Victoir, 2010] *Let $(\mathbf{X}_t)_{t \in [0, T]}$ be a continuous, \mathcal{H} -valued path of bounded variation. Then, the concatenated signature over intervals $[s, u]$ and $[u, t]$ satisfies*

$$\mathbf{Sig}(\mathbf{X})_{st} = \mathbf{Sig}(\mathbf{X})_{su} \otimes \mathbf{Sig}(\mathbf{X})_{ut},$$

for each $0 \leq s \leq u \leq t \leq T$. This identity can be equivalently expressed as follows:

$$\langle \mathbf{Sig}(\mathbf{X})_{st}, \mathbf{w} \rangle = \sum_{\mathbf{uv}=\mathbf{w}} \langle \mathbf{Sig}(\mathbf{X})_{su}, \mathbf{u} \rangle \langle \mathbf{Sig}(\mathbf{X})_{ut}, \mathbf{v} \rangle,$$

where \mathbf{w} is an arbitrary word from \mathbf{W} and \mathbf{uv} is concatenation of the words \mathbf{u} and \mathbf{v} .

In general, if the signatures of two paths of bounded variation are equal, then the paths are equal up to tree-like equivalence [Hambly and Lyons, 2010]. The uniqueness of signatures for time-extended semi-martingales was proved in [Cuchiero et al., 2023]. Here, we state a theorem about the uniqueness of signatures over geometric rough paths of time-extended paths. The proof of this theorem can be found in [Ali and Feng, 2025]. This is the key result for using the signature as a feature map that can universally approximate functions of the underlying path, provided some additional assumptions are satisfied.

Lemma 2.9 (Uniqueness of the signature). *Let $\mathbf{X}, \mathbf{Y} : [0, T] \rightarrow \mathbb{R}^d$ be continuous α -Hölder paths with $\mathbf{X}_0 = \mathbf{Y}_0 = 0$ for some $\alpha > \frac{1}{4}$. Form the time-augmented paths $\widehat{\mathbf{X}}(t) := (t, \mathbf{X}_t)$ and $\widehat{\mathbf{Y}}(t) := (t, \mathbf{Y}_t)$ in \mathbb{R}^{1+d} . Assume their (geometric) terminal signatures coincide at all levels i.e.,*

$$\mathbf{Sig}(\widehat{\mathbf{X}})_{0, T} = \mathbf{Sig}(\widehat{\mathbf{Y}})_{0, T}.$$

Then $\mathbf{X}_t = \mathbf{Y}_t$ for all $t \in [0, T]$.

Before defining a signature kernel, let us define what a static kernel is.

Definition 2.10 (Kernel). Consider a non-empty set \mathcal{X} and some inputs $x, x' \in \mathcal{X}$. The function $\mathbf{K} : \mathcal{X} \times \mathcal{X} \rightarrow \mathbb{R}$ is a kernel if there is a map $\phi : \mathcal{X} \rightarrow \mathcal{H}$ for some Hilbert space \mathcal{H} such that

$$\mathbf{K}(x, x') := \langle \phi(x), \phi(x') \rangle_{\mathcal{H}}, \quad \forall x, x' \in \mathcal{X}.$$

Example 2.11 (Linear Kernel). *The linear kernel between a set of data points $x, y \in \mathbb{R}^d$ is simply the inner product of the two inputs*

$$\mathbf{K}(x, y) = \langle x, y \rangle_{\mathbb{R}^d}.$$

Definition 2.12 (Reproducing Kernel Hilbert Space). A Hilbert space \mathcal{H} of real-valued functions on a set Ω is a *reproducing-kernel Hilbert space (RKHS)* iff there exists, for every $x \in \Omega$, a representer $\mathbf{K}_x \in \mathcal{H}$ such that

$$\langle f, \mathbf{K}_x \rangle_{\mathcal{H}} = f(x), \quad \forall f \in \mathcal{H}.$$

Definition 2.13 (Signature Kernel). [Király and Oberhauser, 2019] For paths $(\mathbf{X}_t)_{t \in [0, T]}$ and $(\mathbf{Y}_t)_{t \in [0, T]}$ in \mathcal{X} , a positive definite static kernel $\mathbf{K} : \mathcal{X} \times \mathcal{X} \rightarrow \mathbb{R}$ with associated RKHS \mathcal{H} . We lift each path $\mathbf{X}, \mathbf{Y} : [0, T] \rightarrow \mathcal{X}$ to the RKHS-valued path

$$\mathbf{K}_X(t) := \mathbf{K}(X_t, \cdot) \in \mathcal{H}.$$

Let $\mathbf{Sig}(\mathbf{K}_X)$ and $\mathbf{Sig}(\mathbf{K}_Y)$ be the signatures of the lifted paths, then the signature kernel is defined as

$$\mathbf{K}_{\mathbf{Sig}}(\mathbf{X}, \mathbf{Y}) := \langle \mathbf{Sig}(\mathbf{K}_X), \mathbf{Sig}(\mathbf{K}_Y) \rangle_{T((\mathcal{H}))},$$

where the inner product is taken over the space $T((\mathcal{H}))$.

Remark 2.14. If the paths \mathbf{X}_t and \mathbf{Y}_t take values in \mathbb{R}^d then the signature kernel can simply be defined as the inner product of the signatures of \mathbf{X}_t and \mathbf{Y}_t i.e.,

$$\mathbf{K}_{\mathbf{Sig}}(\mathbf{X}, \mathbf{Y}) := \langle \mathbf{Sig}(\mathbf{X}), \mathbf{Sig}(\mathbf{Y}) \rangle_{T((\mathbb{R}^d))}.$$

Unless otherwise stated, all paths in our consideration will take values in \mathbb{R}^d for some $d \geq 1$. Also, for our numerical experiments, we will be working with truncated signature kernel which is defined as the scalar product of the truncated signatures of the paths \mathbf{X}_t and \mathbf{Y}_t i.e.,

$$\mathbf{K}_{\mathbf{Sig}}^N(\mathbf{X}, \mathbf{Y}) := \langle \mathbf{Sig}^N(\mathbf{X}), \mathbf{Sig}^N(\mathbf{Y}) \rangle_{T^N(\mathbb{R}^d)}.$$

Let us talk about some normalizations and path extensions required before and after applying signature transform.

2.1. Signature normalizations and path extensions and augmentations.

Definition 2.15 (Robust signatures). Let $\mathbf{X}_1, \dots, \mathbf{X}_n$ be paths taking values in \mathbb{R}^d , and let $\mathbf{Sig}^m(\mathbf{X}_i)$ denote the signature of \mathbf{X}_i truncated at level m . We flatten each truncated signature into a vector by collecting all signature coordinates indexed by words of length at most m . Thus,

$$S_i := \mathbf{Sig}^m(\mathbf{X}_i) \in \mathbb{R}^M,$$

where $M = \sum_{k=0}^m d^k$ is the total number of signature components up to level m . We collect the flattened signatures into the matrix

$$S = \begin{bmatrix} S_1^\top \\ S_2^\top \\ \vdots \\ S_n^\top \end{bmatrix} \in \mathbb{R}^{n \times M}.$$

For each coordinate $j = 1, \dots, M$, define the column-wise median by

$$\mu_j = \text{median}\{S_{1j}, S_{2j}, \dots, S_{nj}\},$$

and define the column-wise inter-quartile range by

$$\text{IQR}_j = Q_{0.75}\{S_{1j}, S_{2j}, \dots, S_{nj}\} - Q_{0.25}\{S_{1j}, S_{2j}, \dots, S_{nj}\}.$$

The robust signature matrix is defined coordinate-wise by

$$(S_{\text{robust}})_{ij} = \frac{S_{ij} - \mu_j}{\text{IQR}_j}, \quad i = 1, \dots, n, \quad j = 1, \dots, M.$$

Equivalently,

$$S_{\text{robust}} = \frac{S - \mu}{\text{IQR}},$$

where the subtraction and division are understood column-wise.

Example 2.16 (RBF Kernel). For $x, y \in \mathbb{R}^d$, we define the RBF kernel using the squared Euclidean distance $\|x - y\|_2^2$ and a positive parameter $\sigma > 0$ as follows:

$$\mathbf{K}(x, y) = \exp\left(-\frac{\|x - y\|_2^2}{2\sigma^2}\right).$$

Definition 2.17 (Positive definite kernel). Let X be a nonempty set. A symmetric kernel

$$\mathbf{K} : X \times X \rightarrow \mathbb{R}$$

is said to be positive definite if, for every $n \in \mathbb{N}$, every choice of points $x_1, \dots, x_n \in X$, and every choice of coefficients $c_1, \dots, c_n \in \mathbb{R}$, we have

$$\sum_{i=1}^n \sum_{j=1}^n c_i c_j \mathbf{K}(x_i, x_j) > 0.$$

Theorem 2.18 (Moore–Aronszajn theorem). Let X be a nonempty set, and let

$$\mathbf{K} : X \times X \rightarrow \mathbb{R}$$

be a symmetric positive definite kernel. Then there exists a unique Hilbert space $\mathcal{H}_{\mathbf{K}}$ of functions $f : X \rightarrow \mathbb{R}$ such that \mathbf{K} is the reproducing kernel of $\mathcal{H}_{\mathbf{K}}$.

Definition 2.19 (Minimum-norm interpolant). Let Ω be an input domain, and let

$$X = \{x_1, \dots, x_N\} \subset \Omega$$

be a set of distinct data points with corresponding values

$$Y = \{y_1, \dots, y_N\} \subset \mathbb{R}.$$

Let \mathcal{H} be a Hilbert space of functions on Ω . The minimum-norm interpolant associated with the data (X, Y) is defined by

$$f_{X,Y}^* = \arg \min_{f \in \mathcal{H}} \|f\|_{\mathcal{H}} \quad \text{subject to} \quad f(x_i) = y_i, \quad i = 1, \dots, N.$$

Definition 2.20 (Truncated RBF signature kernel). Let \mathbf{X} and \mathbf{Y} be paths in \mathbb{R}^d , and let $\mathbf{Sig}^m(\mathbf{X})$ and $\mathbf{Sig}^m(\mathbf{Y})$ denote their signatures truncated up to level m . After flattening the truncated signatures into vectors, we define the truncated RBF signature kernel by

$$\mathbf{K}_{\text{RBF-sig}}^m(\mathbf{X}, \mathbf{Y}) = \exp\left(-\frac{\|\mathbf{Sig}^m(\mathbf{X}) - \mathbf{Sig}^m(\mathbf{Y})\|_2^2}{2\sigma^2}\right), \quad \sigma > 0.$$

Equivalently, using the Euclidean inner product on the flattened truncated signature vectors, we can write

$$\mathbf{K}_{\text{RBF-sig}}^m(\mathbf{X}, \mathbf{Y}) = \exp\left(-\frac{\|\mathbf{Sig}^m(\mathbf{X})\|_2^2 + \|\mathbf{Sig}^m(\mathbf{Y})\|_2^2 - 2\langle \mathbf{Sig}^m(\mathbf{X}), \mathbf{Sig}^m(\mathbf{Y}) \rangle}{2\sigma^2}\right).$$

Definition 2.21 (Linear signature kernel Gram matrix). Let $\mathbf{X}_1, \dots, \mathbf{X}_n$ be paths in \mathbb{R}^d , and let

$$S_i = \mathbf{Sig}^m(\mathbf{X}_i) \in \mathbb{R}^M, \quad i = 1, \dots, n,$$

denote their flattened signatures truncated up to level m . We collect these vectors row-wise in the matrix

$$S = \begin{bmatrix} S_1^\top \\ S_2^\top \\ \vdots \\ S_n^\top \end{bmatrix} \in \mathbb{R}^{n \times M}.$$

The linear signature kernel Gram matrix is defined by

$$\mathbb{K} = SS^\top \in \mathbb{R}^{n \times n}.$$

Equivalently, its entries are given by

$$\mathbb{K}_{ij} = \langle S_i, S_j \rangle_{\mathbb{R}^M} = \langle \mathbf{Sig}^m(\mathbf{X}_i), \mathbf{Sig}^m(\mathbf{X}_j) \rangle, \quad i, j = 1, \dots, n.$$

Definition 2.22 (RBF signature kernel Gram matrix). Using the signature feature matrix S , the RBF signature kernel Gram matrix $\mathbb{K} \in \mathbb{R}^{n \times n}$ is defined by

$$\mathbb{K}_{ij} = \exp\left(-\frac{\|S_i\|_2^2 + \|S_j\|_2^2 - 2\langle S_i, S_j \rangle_{\mathbb{R}^M}}{2\sigma^2}\right), \quad i, j = 1, \dots, n,$$

where S_i and S_j denote the i -th and j -th rows of S , and $\sigma > 0$.

2.2. Sampling methods.

Definition 2.23 (Count-sampling method). Let $X = (X^1, \dots, X^d) : [0, T] \rightarrow \mathbb{R}^d$ be a path discretized at N points $0, x_1, \dots, x_{N-1} = T$, and write X_{0, x_j} for the restriction of X to the prefix interval $[0, x_j]$. The count-sampling construction produces the family of N nested training paths

$$X_0 := X_{t_0, t_0}, \quad X_1 := X_{0, t_1}, \quad \dots, \quad X_N := X_{0, T}.$$

The first sample X_0 is the degenerate two-point path $(X(0), X(0))$ formed by repeating the initial value of X , so that X_0 has at least two values and the signature kernel is well-defined on it. This convention lets the initial point of the system be treated uniformly with the longer prefixes and is needed by the algorithms introduced below.

Remark 2.24. All count-sampled paths X_0, \dots, X_{N-1} share the starting point $X(0)$ but differ in length: X_j is supported on $[0, t_j]$ and contains strictly more path-dependent information than its predecessors. From a single observed time series we therefore produce a hierarchical training set of N nested paths, ideally suited as inputs to the signature kernel K_{sig} . Throughout the rest of the section, every reference to “training paths X_0, \dots, X_{N-1} ” should be understood as referring to this construction.

Count Method Speedup. When using the count-sampling method, one can exploit Chen’s identity to greatly improve computational cost. Two popular signature libraries, `keras-sig` and `signatory`, both expose this speedup through the `stream` argument of their signature-computation routines, and both support GPU acceleration; we therefore rely on these libraries in our numerical sections.

Suppose we use the count-sampling method to generate N nested training paths X_0, X_1, \dots, X_{N-1} , each of dimension d . The j -th path has length

$$L_j = \begin{cases} 2, & j = 0, \\ j + 1, & j \geq 1. \end{cases}$$

We set $L_0 = 2$ so that even the shortest training path admits a well-defined truncated signature; this convention is immaterial for the asymptotic analysis. (Here N is the number of count-sampled paths used in this section; this corresponds to $N+1$ in the collocation setup of the previous sections, where paths were indexed X_0, \dots, X_N .)

In most numerical libraries, path tensors are specified in the form (B, L, D) , where B is the batch dimension, L is the length of the path, and D is the path dimension. The naive approach therefore produces N separate path tensors of size $(1, L_j, d)$ and calls the signature routine on each independently. By the analysis of [Kidger and Lyons, 2021], computing the truncated signature of a single length- L path to depth M requires a fused tensor-algebra multiplication at cost $O(d^M)$ (treating M as a constant) for each of the $L - 1$ increments, giving total cost $(L - 1) \cdot O(d^M)$ per path. Summing over all N paths:

$$\begin{aligned} \text{total cost} &= \sum_{j=0}^{N-1} (L_j - 1) \cdot O(d^M) = ((L_0 - 1) + \sum_{j=1}^{N-1} (L_j - 1)) \cdot O(d^M) \\ &= (1 + \sum_{j=1}^{N-1} j) \cdot O(d^M) = (1 + \frac{N(N-1)}{2}) \cdot O(d^M) = O(N^2 d^M). \end{aligned}$$

Using the count method speedup, we only pass into the signature function the final prefix path tensor of size $(1, N, d)$. It processes the entire stream from left to right using one fused multiplication per increment, and Chen’s identity that $\mathbf{Sig}^M(X_{[t_0, t_{j+1}]}) = \mathbf{Sig}^M(X_{[t_0, t_j]}) \otimes \mathbf{Sig}^M(X_{[t_j, t_{j+1}]})$ allows the reuse of all previously computed leading increments. The total time complexity is therefore

$$\text{total cost} = (N - 1) \cdot O(d^M) = O(N d^M),$$

an order- N improvement over the naive sum.

Now consider the case in which we aim to compute the truncated signature-kernel Gram matrix of the prefix paths up to depth M . Previous methods either rely on dynamic-programming techniques [Király and Oberhauser, 2019] or on PDE approximations exploiting the fact that the signature kernel satisfies a Goursat PDE [Salvi et al., 2021]; both are implemented efficiently in the Python package `PySigLib`. The Goursat approach has cost $O(N^2 L^2 d)$, and since the maximum path length satisfies $L = N$ in our count-sampled setting, this becomes $O(N^4 d)$. A dynamic-programming approach yields $O(N^2 L^2 M d) = O(N^4 M d)$ for the same $N \times N$ kernel matrix.

With the count speedup, we compute the truncated signature vectors in $O(N d^M)$ time, producing an $N \times C$ matrix of signature vectors S in which row j holds the entries of $\mathbf{Sig}^M(X_j)$ flattened into a vector of length $C = \sum_{k=0}^M d^k = O(d^M)$. To form the kernel Gram matrix we compute $K = S S^\top$, a matrix multiplication taking $O(N^2 d^M)$ time. We conclude with a Gram-matrix runtime of $O(N^2 d^M)$, in which the matrix multiplication dominates the signature-computation step.

The runtime for both signature computations and signature-kernel Gram-matrix computations are summarized in Table 1 and Table 2, respectively. The Goursat and dynamic-programming methods inherit only a linear d -dependence from the static-kernel evaluations they invoke. The count method, by contrast, materializes the full truncated signature vector of length $O(d^M)$ and pays for it explicitly in the Gram matrix multiplication. The two regimes therefore exchange a quartic N^4 scaling for an exponential d^M scaling — a favorable trade-off whenever

$$N \gtrsim d^{(M-1)/2},$$

obtained by equating $N^4 d$ with $N^2 d^M$. Our experiments operate in the regime where N is large and M is small — the branched signature framework lets us extract sufficient path-wise information at low truncation depth — so the $N^4 \rightarrow N^2$ improvement dominates the unfavorable $d \rightarrow d^M$ trade-off. This regime is exactly the one encountered in time-series data-driven modeling, where long observation records produce many nested prefix paths but only modest signature depth is needed, and the count-method speedup is therefore decisive.

2.3. Signature kernel for geometric rough path. In this subsection, we define the signature kernel for geometric rough paths. Previously, signature kernels were defined for paths of bounded variation. In general, α -Hölder paths with $\alpha > \frac{1}{4}$ admit geometric rough path lifts, and by Lyons’ extension theorem [Friz and Victoir, 2010], the signatures of these lifts are well-defined at all higher levels. This allows us to define the signature kernel for such geometric rough paths as follows.

Method	Time
Naive (independent calls)	$O(N^2 d^M)$
Count method	$O(N d^M)$

TABLE 1. Runtime comparison for computing all N truncated signature vectors to depth M for the count-sampled prefix paths X_0, \dots, X_{N-1} of dimension d . The naive case calls `signature()` independently on each path tensor of size $(1, L_j, d)$. The stream case passes a single tensor of size $(1, N, d)$ with `stream=True`.

Method	Time
Goursat PDE	$O(N^4 d)$
Dynamic programming	$O(N^4 M d)$
Count method	$O(N^2 d^M)$

TABLE 2. Runtime comparison for computing the $N \times N$ truncated signature kernel Gram matrix $K_{ij} = \langle \mathbf{Sig}^M(X_i), \mathbf{Sig}^M(X_j) \rangle$ for the count-sampled prefix paths. N denotes the number of paths, $L \leq N$ the maximum path length, d the path dimension, and M the truncation depth. (Note $L=N$)

Definition 2.25 (Signature Kernel for a geometric rough path). [Király and Oberhauser, 2019] Let $(\mathbf{X}_t)_{t \in [0, T]}$ and $(\mathbf{Y}_t)_{t \in [0, T]}$ be α -Hölder paths for $\alpha > \frac{1}{4}$ taking values in \mathbb{R}^d , and let $\mathbf{Sig}(\mathbf{X})$ and $\mathbf{Sig}(\mathbf{Y})$ be their signatures defined by Lyons' extension theorem. The signature kernel $\mathbf{K}_{\mathbf{Sig}}(\mathbf{X}, \mathbf{Y})$ for these paths is defined as

$$\mathbf{K}_{\mathbf{Sig}}(\mathbf{X}, \mathbf{Y}) := \langle \mathbf{Sig}(\mathbf{X}), \mathbf{Sig}(\mathbf{Y}) \rangle_{T((\mathbb{R}^d))},$$

where

$$\langle \mathbf{Sig}(\mathbf{X}), \mathbf{Sig}(\mathbf{Y}) \rangle_{T((\mathbb{R}^d))} := \sum_{n=0}^{\infty} \langle \pi_n(\mathbf{Sig}(\mathbf{X})), \pi_n(\mathbf{Sig}(\mathbf{Y})) \rangle_{(\mathbb{R}^d)^{\otimes n}},$$

whenever the series is well-defined. Here

$$\pi_n(\mathbf{Sig}(\mathbf{X})) \in (\mathbb{R}^d)^{\otimes n}$$

denotes the signature component of level- n .

Equivalently, if $\mathbf{w} = w_1 \dots w_n$ is a word of length n from the set of words \mathbf{W} , then

$$\mathbf{K}_{\mathbf{Sig}}(\mathbf{X}, \mathbf{Y}) = \sum_{n=0}^{\infty} \sum_{|\mathbf{w}|=n} \langle \mathbf{Sig}(\mathbf{X}), \mathbf{w} \rangle \langle \mathbf{Sig}(\mathbf{Y}), \mathbf{w} \rangle.$$

Next, we are going to state and prove universal approximation theorem for the signature kernel defined over a geometric rough path. We will be leveraging the universal approximation theorem for the signature of geometric rough path.

Theorem 2.26 (Universal approximation theorem for signature kernel). *Let \mathcal{K} be the compact set of paths that admit a geometric rough path lift i.e.,*

$$\mathcal{K} \subset \left\{ \mathbf{X} : [0, T] \rightarrow \mathbb{R}^d \text{ such that } \mathbf{X} \text{ admits a geometric rough path lift} \right\}.$$

Define the compact set of time extended paths $\widehat{\mathcal{K}}$ as

$$\widehat{\mathcal{K}} \subset \left\{ \widehat{\mathbf{X}}_t := (t, \mathbf{X}_t) \text{ such that } \mathbf{X}_t \in \mathcal{K} \right\}.$$

Then for every continuous function $f(\widehat{\mathcal{K}}; \mathbb{R})$ and every $\epsilon > 0$, there exist an integer $N \geq 0$, paths $\widehat{\mathbf{Y}}^1, \dots, \widehat{\mathbf{Y}}^M \in \widehat{\mathcal{K}}$, and scalars $\alpha_1, \dots, \alpha_M$ such that

$$\sup_{\widehat{\mathbf{X}} \in \widehat{\mathcal{K}}} \left| f(\mathbf{Sig}^p(\widehat{\mathbf{X}})) - \sum_{i=1}^M \alpha_i \mathbf{K}_{\mathbf{Sig}}^N(\widehat{\mathbf{X}}, \widehat{\mathbf{Y}}^i) \right| < \epsilon,$$

where $\mathbf{Sig}^p(\widehat{\mathbf{X}})$ is the geometric rough path lift of $\widehat{\mathbf{X}}$ for some $p \in \mathbb{N}$ depending on the Hölder regularity of \mathbf{X} .

Proof. Leveraging the universal approximation theorem for signatures of geometric rough paths [Ali and Feng, 2025], we have that for every $f \in C(\widehat{\mathcal{K}}; \mathbb{R})$ and every $\varepsilon > 0$, there exist $N \geq 0$ and $\ell \in T^{(N)}(\mathbb{R}^{d+1})$ such that

$$\sup_{\widehat{\mathbf{X}} \in \widehat{\mathcal{K}}} \left| f\left(\mathbf{Sig}^p(\widehat{\mathbf{X}})\right) - \left\langle \mathbf{Sig}^N(\widehat{\mathbf{X}}), \ell \right\rangle \right| < \varepsilon. \quad (2.1)$$

Now, let

$$M_N := \text{span} \left\{ \mathbf{Sig}^N(\widehat{\mathbf{Y}}) : \widehat{\mathbf{Y}} \in \widehat{\mathcal{K}} \right\} \subset T^{(N)}(\mathbb{R}^{d+1}).$$

Let \mathcal{P}_{M_N} be the orthogonal projection onto M_N , and define

$$\ell_N := \mathcal{P}_{M_N} \ell.$$

For every $\widehat{\mathbf{X}} \in \widehat{\mathcal{K}}$, we have

$$\mathbf{Sig}^N(\widehat{\mathbf{X}}) \in M_N.$$

Therefore,

$$\left\langle \mathbf{Sig}^N(\widehat{\mathbf{X}}), \ell \right\rangle = \left\langle \mathbf{Sig}^N(\widehat{\mathbf{X}}), \mathcal{P}_{M_N} \ell \right\rangle = \left\langle \mathbf{Sig}^N(\widehat{\mathbf{X}}), \ell_N \right\rangle.$$

Since $\ell_N \in M_N$, by the definition of M_N , there exist $\widehat{\mathbf{Y}}^1, \dots, \widehat{\mathbf{Y}}^M \in \widehat{\mathcal{K}}$ and scalars $\alpha_1, \dots, \alpha_M \in \mathbb{R}$ such that

$$\ell_N = \sum_{i=1}^M \alpha_i \mathbf{Sig}^N(\widehat{\mathbf{Y}}^i).$$

Hence, for every $\widehat{\mathbf{X}} \in \widehat{\mathcal{K}}$,

$$\begin{aligned} \left\langle \mathbf{Sig}^N(\widehat{\mathbf{X}}), \ell \right\rangle &= \left\langle \mathbf{Sig}^N(\widehat{\mathbf{X}}), \ell_N \right\rangle \\ &= \left\langle \mathbf{Sig}^N(\widehat{\mathbf{X}}), \sum_{i=1}^M \alpha_i \mathbf{Sig}^N(\widehat{\mathbf{Y}}^i) \right\rangle \\ &= \sum_{i=1}^M \alpha_i \left\langle \mathbf{Sig}^N(\widehat{\mathbf{X}}), \mathbf{Sig}^N(\widehat{\mathbf{Y}}^i) \right\rangle \\ &= \sum_{i=1}^M \alpha_i \mathbf{K}_{\mathbf{Sig}}^N(\widehat{\mathbf{X}}, \widehat{\mathbf{Y}}^i). \end{aligned}$$

Combining this identity with (2.1) gives

$$\sup_{\widehat{\mathbf{X}} \in \widehat{\mathcal{K}}} \left| f\left(\mathbf{Sig}^p(\widehat{\mathbf{X}})\right) - \sum_{i=1}^M \alpha_i \mathbf{K}_{\mathbf{Sig}}^N(\widehat{\mathbf{X}}, \widehat{\mathbf{Y}}^i) \right| < \varepsilon.$$

This proves the theorem. \square

3. BRANCHED SIGNATURE KERNEL

In this section we are going to define branched signature kernel. To begin with, let us define a Hopf algebra and Connes–Kreimer Hopf algebra of rooted trees, a special example of Hopf algebra where branched signature lives.

A Hopf algebra \mathcal{H} is an algebraic structure that contains a product $\cdot : \mathcal{H} \otimes \mathcal{H} \rightarrow \mathcal{H}$, which tells how to combine two objects; a coproduct $\Delta : \mathcal{H} \rightarrow \mathcal{H} \otimes \mathcal{H}$, which tells how to split an object; and an antipode $\mathcal{S} : \mathcal{H} \rightarrow \mathcal{H}$, which is the way to encode inverses. Let \mathcal{H}^* be the dual of \mathcal{H} . The product \star on the dual space \mathcal{H}^* is defined via coproduct on \mathcal{H} as

$$\langle f \star g, h \rangle = \langle f \otimes g, \Delta h \rangle,$$

for any $f, g \in \mathcal{H}^*$ and $h \in \mathcal{H}$.

The Connes–Kreimer Hopf algebra of rooted trees is a special type of Hopf algebra which is used in the setting of branched rough paths and branched signatures. The iterated integrals for geometric rough paths are encoded by words \mathbf{w} made from the alphabet $\mathcal{A} = \{1, 2, \dots, d\}$. However, in the case of branched rough paths, the iterated integrals are encoded by decorated rooted trees, with decorations coming from the set \mathcal{A} . For instance, the iterated integral

$$\int_s^t \left(\int_s^u d\mathbf{X}_r^i \right) \left(\int_s^u d\mathbf{X}_r^j \right) d\mathbf{X}_u^k$$

is encoded by the tree

$$\mathbb{V}_k^{i,j}.$$

The Connes–Kreimer Hopf algebra of rooted trees \mathcal{H} [Connes and Kreimer, 1999] is the polynomial algebra in which rooted trees play the role of variables. The product of trees is given by placing trees side by side to form a forest, while the coproduct is given by all possible ways of cutting a tree into smaller trees. The Connes–Kreimer Hopf algebra of rooted trees \mathcal{H} is the appropriate algebraic structure in which the branched signature lives. The definition of the branched signature follows.

Definition 3.1 (Branched Signature). [Gubinelli, 2010] Let $\mathcal{A} = \{1, \dots, d\}$ be an alphabet set corresponding to a given d -dimensional path $\mathbf{X} : [0, T] \rightarrow \mathbb{R}^d$. Let \mathcal{T} be the set of rooted trees with vertices decorated by letters in \mathcal{A} . Let \mathcal{H} be the Connes–Kreimer Hopf algebra of rooted trees generated by trees in \mathcal{T} , with product given by disjoint union of forests and unit $\mathbf{1}$. We define *branched signature* of \mathbf{X} as a functional on \mathcal{H} given by

$$\mathbf{BSig}(\mathbf{X})_{st} = \sum_{\tau \in \mathcal{T}, |\tau| \leq N} \langle \mathbf{BSig}(\mathbf{X})_{st}, \tau \rangle \mathbf{e}_\tau, \quad (3.1)$$

where for each $\tau \in \mathcal{H}$ the component $\langle \mathbf{BSig}(\mathbf{X})_{st}, \tau \rangle$ of the branched signature is recursively defined as

$$\langle \mathbf{BSig}(\mathbf{X})_{st}, \mathbf{1} \rangle = 1, \quad \text{and} \quad \langle \mathbf{BSig}(\mathbf{X})_{st}, \tau \rangle = \int_s^t \langle \mathbf{BSig}(\mathbf{X})_{su}, \tau' \rangle d\mathbf{x}_u^{\mathbf{r}},$$

where τ is the tree that we get by grafting the root vertex \mathbf{r} to τ' i.e., $\tau = [\tau']_{\mathbf{r}}$.

Definition 3.2 (Branched signature kernel). Let $(\mathbf{X}_t)_{t \in [0, T]}$ and $(\mathbf{Y}_t)_{t \in [0, T]}$ be α -Hölder paths for $\alpha > \frac{1}{4}$ taking values in \mathbb{R}^d . Let $\mathbf{BSig}(\mathbf{X})$ and $\mathbf{BSig}(\mathbf{Y})$ denote their branched signatures, whose components are indexed by decorated rooted forests in the Connes–Kreimer Hopf algebra \mathcal{H} . The branched signature kernel $\mathbf{K}_{\mathbf{BSig}}(\mathbf{X}, \mathbf{Y})$ is defined as

$$\mathbf{K}_{\mathbf{BSig}}(\mathbf{X}, \mathbf{Y}) := \langle \mathbf{BSig}(\mathbf{X}), \mathbf{BSig}(\mathbf{Y}) \rangle_{\mathcal{H}^*},$$

where

$$\langle \mathbf{BSig}(\mathbf{X}), \mathbf{BSig}(\mathbf{Y}) \rangle_{\mathcal{H}^*} := \sum_{n=0}^{\infty} \langle \pi_n(\mathbf{BSig}(\mathbf{X})), \pi_n(\mathbf{BSig}(\mathbf{Y})) \rangle_{\mathcal{H}_n^*},$$

whenever the series makes sense. Also,

$$\pi_n(\mathbf{BSig}(\mathbf{X})) \in \mathcal{H}_n^*$$

denotes the degree- n component of the branched signature and \mathcal{H}_n^* denotes the dual of the space spanned by decorated rooted forests with exactly n vertices.

Equivalently, if \mathcal{F}_n denotes the set of decorated rooted forests of degree n , then

$$\mathbf{K}_{\mathbf{BSig}}(\mathbf{X}, \mathbf{Y}) = \sum_{n=0}^{\infty} \sum_{\tau \in \mathcal{F}_n} \langle \mathbf{BSig}(\mathbf{X}), \tau \rangle \langle \mathbf{BSig}(\mathbf{Y}), \tau \rangle.$$

Theorem 3.3 (Universal approximation theorem for branched signature kernel). *Let \mathcal{K} be the compact subset of paths that admit a branched rough path lift i.e.,*

$$\mathcal{K} \subset \left\{ \mathbf{X} : [0, T] \rightarrow \mathbb{R}^d \text{ such that } \mathbf{X} \text{ admits a branched rough path lift} \right\}.$$

Define the compact set of time extended paths $\widehat{\mathcal{K}}$ as

$$\widehat{\mathcal{K}} \subset \left\{ \widehat{\mathbf{X}}_t := (t, \mathbf{X}_t) \text{ such that } \mathbf{X}_t \in \mathcal{K} \right\}.$$

Then for every continuous function $f(\widehat{\mathcal{K}}; \mathbb{R})$ and every $\epsilon > 0$, there exist an integer $N \geq 0$, paths $\widehat{\mathbf{Y}}^1, \dots, \widehat{\mathbf{Y}}^M \in \widehat{\mathcal{K}}$, and scalars $\alpha_1, \dots, \alpha_M$ such that

$$\sup_{\widehat{\mathbf{X}} \in \widehat{\mathcal{K}}} \left| f\left(\mathbf{BSig}^p(\widehat{\mathbf{X}})\right) - \sum_{i=1}^M \alpha_i \mathbf{K}_{\mathbf{BSig}}^N(\widehat{\mathbf{X}}, \widehat{\mathbf{Y}}^i) \right| < \epsilon,$$

where $\mathbf{BSig}^p(\widehat{\mathbf{X}})$ is the branched rough path lift of $\widehat{\mathbf{X}}$ for some $p \in \mathbb{N}$ depending on the Hölder regularity of \mathbf{X} .

Proof. Using the universal approximation theorem for signatures of branched rough paths [Ali and Feng, 2025], we have that for every $f \in C(\widehat{\mathcal{K}}; \mathbb{R})$ and every $\epsilon > 0$, there exist $N \geq 0$ and $\tau \in \mathcal{H}$ such that

$$\sup_{\widehat{\mathbf{X}} \in \widehat{\mathcal{K}}} \left| f\left(\mathbf{BSig}^p(\widehat{\mathbf{X}})\right) - \left\langle \mathbf{BSig}^N(\widehat{\mathbf{X}}), \tau \right\rangle \right| < \epsilon, \quad (3.2)$$

where \mathcal{H} is the Hopf algebra of decorated rooted trees with the decoration coming from $\mathcal{A} \cup \{0\}$ with $\mathcal{A} := \{1, 2, \dots, d\}$ and 0 is corresponding to time component. Now, let

$$M_N := \text{span} \left\{ \mathbf{BSig}^N(\widehat{\mathbf{Y}}) : \widehat{\mathbf{Y}} \in \widehat{\mathcal{K}} \right\} \subset \mathcal{H}^*.$$

Let \mathcal{P}_{M_N} be the orthogonal projection onto M_N , and define

$$\tau_N := \mathcal{P}_{M_N} \tau.$$

For every $\widehat{\mathbf{X}} \in \widehat{\mathcal{K}}$, we have

$$\mathbf{BSig}^N(\widehat{\mathbf{X}}) \in M_N.$$

Therefore,

$$\left\langle \mathbf{BSig}^N(\widehat{\mathbf{X}}), \tau \right\rangle = \left\langle \mathbf{BSig}^N(\widehat{\mathbf{X}}), \mathcal{P}_{M_N} \tau \right\rangle = \left\langle \mathbf{BSig}^N(\widehat{\mathbf{X}}), \tau_N \right\rangle.$$

Since $\tau_N \in M_N$, by the definition of M_N , there exist $\widehat{\mathbf{Y}}^1, \dots, \widehat{\mathbf{Y}}^M \in \widehat{\mathcal{K}}$ and scalars $\alpha_1, \dots, \alpha_M \in \mathbb{R}$ such that

$$\tau_N = \sum_{i=1}^M \alpha_i \mathbf{BSig}^N(\widehat{\mathbf{Y}}^i).$$

Hence, for every $\widehat{\mathbf{X}} \in \widehat{\mathcal{K}}$,

$$\begin{aligned} \left\langle \mathbf{BSig}^N(\widehat{\mathbf{X}}), \tau \right\rangle &= \left\langle \mathbf{BSig}^N(\widehat{\mathbf{X}}), \tau_N \right\rangle \\ &= \left\langle \mathbf{BSig}^N(\widehat{\mathbf{X}}), \sum_{i=1}^M \alpha_i \mathbf{BSig}^N(\widehat{\mathbf{Y}}^i) \right\rangle \\ &= \sum_{i=1}^M \alpha_i \left\langle \mathbf{BSig}^N(\widehat{\mathbf{X}}), \mathbf{BSig}^N(\widehat{\mathbf{Y}}^i) \right\rangle \\ &= \sum_{i=1}^M \alpha_i \mathbf{K}_{\mathbf{BSig}}^N(\widehat{\mathbf{X}}, \widehat{\mathbf{Y}}^i). \end{aligned}$$

Combining this identity with (3.2) gives

$$\sup_{\widehat{\mathbf{X}} \in \widehat{\mathcal{K}}} \left| f\left(\mathbf{BSig}^p(\widehat{\mathbf{X}})\right) - \sum_{i=1}^M \alpha_i \mathbf{K}_{\mathbf{BSig}}^N(\widehat{\mathbf{X}}, \widehat{\mathbf{Y}}^i) \right| < \varepsilon.$$

This proves the claim. \square

Instead of computing the branched signature kernel of the paths \mathbf{X} and \mathbf{Y} , we compute the geometric signature kernel of the extended paths $\bar{\mathbf{X}}$ and $\bar{\mathbf{Y}}$ and leverage the Hairer–Kelly morphism [Hairer and Kelly, 2015] to show that the geometric signature kernel of extended paths gives the information that a branched signature kernel contains.

The Hairer–Kelly morphism Ψ is a Hopf algebra morphism from the Connes–Kreimer Hopf algebra of rooted trees \mathcal{H} to shuffle Hopf algebra over vector space \mathcal{V} spanned by rooted trees i.e.,

$$\Psi : (\mathcal{H}, \cdot, \Delta) \rightarrow (T(\mathcal{V}), \sqcup, \bar{\Delta}).$$

For a tree $\tau \in \mathcal{F}_n$, the morphism Ψ is defined as

$$\Psi(\tau) = \tau + \Psi_{n-1}(\tau),$$

where $\Psi_{n-1}(\tau)$ is all the smaller trees coming from cutting the tree τ in all possible ways.

The existence of such a morphism Ψ and the extended path $\bar{\mathbf{X}}$ is proved in [Hairer and Kelly, 2015]. The main theorem in the paper states that for a branched rough path $\mathbf{BSig}^N(\mathbf{X})$, one can construct the extended path $\bar{\mathbf{X}}$ and the geometric rough path $\mathbf{Sig}^N(\mathbf{X})$ such that

$$\langle \mathbf{BSig}^N(\mathbf{X})_{st}, \tau \rangle = \langle \mathbf{Sig}^N(\bar{\mathbf{X}})_{st}, \Psi(\tau) \rangle,$$

for all $\tau \in \mathcal{F}_n$.

This result can also be applied to branched and geometric signatures using the extension theorems from rough paths to signatures. Finally, we state and prove the universal approximation theorem that claims that any function of the branched rough path can be approximated by the signature kernel of the extended paths. The precise statement and proof of the theorem are given as follows.

Theorem 3.4 (Universal approximation theorem for signature kernel of extended paths). *Let \mathcal{K} be the compact subset of time-extended paths that admit a branched rough path lift i.e.,*

$$\mathcal{K} \subset \left\{ \mathbf{X} : [0, T] \rightarrow \mathbb{R}^{d+1} \text{ such that } \mathbf{X} = (t, \mathbf{X}^-) \text{ and } \mathbf{X}^- \text{ admits a branched rough path lift} \right\}.$$

Then for every continuous function $f(\mathcal{K}; \mathbb{R})$ and every $\varepsilon > 0$, there exist an integer $N \geq 0$, paths $\mathbf{Y}^1, \dots, \mathbf{Y}^M \in \mathcal{K}$, and scalars $\alpha_1, \dots, \alpha_M$ such that

$$\sup_{\mathbf{X} \in \mathcal{K}} \left| f(\mathbf{BSig}^p(\mathbf{X})) - \sum_{i=1}^M \alpha_i \mathbf{K}_{\Psi, \mathbf{Sig}}^N(\bar{\mathbf{X}}, \bar{\mathbf{Y}}^i) \right| < \varepsilon,$$

where $\mathbf{BSig}^p(\mathbf{X})$ is the branched rough path lift of \mathbf{X} for some $p \in \mathbb{N}$ depending on the Hölder regularity of \mathbf{X}^- , $\bar{\mathbf{X}}, \bar{\mathbf{Y}}^i$ are the extended paths constructed via extension map of Hairer-Kelly, and $\mathbf{K}_{\Psi, \mathbf{Sig}}^N(\bar{\mathbf{X}}, \bar{\mathbf{Y}}^i)$ is defined as

$$\mathbf{K}_{\Psi, \mathbf{Sig}}^N(\bar{\mathbf{X}}, \bar{\mathbf{Y}}^i) := \sum_{n=0}^N \sum_{\tau \in \mathcal{F}_n} \langle \mathbf{Sig}(\bar{\mathbf{X}}), \Psi(\tau) \rangle \langle \mathbf{Sig}(\bar{\mathbf{Y}}^i), \Psi(\tau) \rangle.$$

Proof. By the extension of Hairer-Kelly, for a path \mathbf{X} that admits a branched rough path, there exists a map Ψ and an extended path $\bar{\mathbf{X}}$ such that each component of the branched signature corresponding a tree $\tau \in \mathcal{H}$ can be identified as the component of signature of $\bar{\mathbf{X}}$ corresponding to $\Psi(\tau) \in T(\mathcal{V})$ i.e.,

$$\langle \mathbf{BSig}(\mathbf{X}), \tau \rangle = \langle \mathbf{Sig}(\bar{\mathbf{X}}), \Psi(\tau) \rangle.$$

This should also be true for truncated signatures. Therefore, for paths \mathbf{X} and \mathbf{Y}_i

$$\begin{aligned} \mathbf{K}_{\mathbf{BSig}}^N(\mathbf{X}, \mathbf{Y}^i) &= \sum_{n=0}^N \sum_{\tau \in \mathcal{F}_n} \langle \mathbf{BSig}(\mathbf{X}), \tau \rangle \langle \mathbf{BSig}(\mathbf{Y}^i), \tau \rangle \\ &= \sum_{n=0}^N \sum_{\tau \in \mathcal{F}_n} \langle \mathbf{Sig}(\bar{\mathbf{X}}), \Psi(\tau) \rangle \langle \mathbf{Sig}(\bar{\mathbf{Y}}^i), \Psi(\tau) \rangle = \mathbf{K}_{\Psi, \mathbf{Sig}}^N(\bar{\mathbf{X}}, \bar{\mathbf{Y}}^i). \end{aligned}$$

Hence, the claim follows by Theorem 3.3. \square

Definition 3.5 (*t*-value lift). Suppose we observe a stream of forcing data $(t, F(t)) \in \mathbb{R}^2$. This stream of data can be lifted into \mathbb{R}^3 by augmenting the path to $(t, F(t), t^\alpha) \in \mathbb{R}^3$ where $\alpha \in (0, 1)$.

The motivation for the *t*-value lift comes from the case where the forcing $F(t)$ is modeled by a fractional Brownian motion (fBm) $\mathbf{B}^H(t)$ with Hurst parameter $H \in (0, \frac{1}{2})$. In this case, the covariance of fBm satisfies

$$\mathbb{E} [\mathbf{B}^H(t) \mathbf{B}^H(t)] = t^{2H}.$$

Thus, the deterministic component t^α can be viewed as a way to encode the covariance related correction associated with the rough forcing. In particular, when $\alpha = 2H$, this lift agrees with the type of extended component appearing in the branched-to-geometric realization used in [Ali and Feng, 2025].

Neural Network Lift: In cases where the form of the driving signal is not known beforehand, one cannot prescribe an explicit path extension by hand. The path following a Brownian motion, fractional Brownian motion, or other rough frameworks would require a different extension framework. We therefore aim to construct an extension in a data dependent way. Neural Network path extensions were first considered in [Kidger et al., 2019] and noted as a way to increase the expressive power of the signature. The general method is mostly applied using convolution layers, recurrent neural networks, and sliding window architectures to lift the path before signatures are taken. In [Ali and Feng, 2025], a neural network lift is applied using an MLP to construct a specific mapping that encodes the branched rough path information before taking signatures. We will apply this framework in our paper.

Definition 3.6 (Neural Network Lift). Let $\mathbf{X}_t : [0, T] \rightarrow \mathbb{R}^{d+1}$ be a time-extended path. We define a trainable map

$$\Phi_\theta : \mathbb{R}^{d+1} \rightarrow \mathbb{R}^m,$$

with learnable parameters θ . The learned coordinates may be defined as

$$\bar{\mathbf{X}}_t^\theta = \Phi_\theta(\mathbf{X}_t) \in \mathbb{R}^m, \quad t \in [0, T].$$

The lifted path is then constructed by concatenating the learned features with the original path

$$\bar{\bar{\mathbf{X}}}_t^\theta = (\mathbf{X}_t, \bar{\mathbf{X}}_t^\theta) \in \mathbb{R}^{d+1+m}, \quad t \in [0, T].$$

The goal is to train for an extension which both improves model loss while staying consistent with the branched framework. We use a shuffle loss which enforces the integration by parts identity. The role of the shuffle loss is to make the learned coordinates $\bar{\bar{\mathbf{X}}}_\theta$ closer to geometric signature coordinates. At second order, this means that the product of two increments should agree with the sum of the two ordered iterated integrals, as in the integration-by-parts identity.

Definition 3.7 (Shuffle Loss). For $a, b \in \{1, \dots, m\}$ and $t_i \in \pi[0, T]$, define

$$D_i^a(\theta) := \bar{\bar{\mathbf{X}}}_\theta^a(t_i) - \bar{\bar{\mathbf{X}}}_\theta^a(t_0), \quad \text{and} \quad I_i^{a,b}(\theta) := \int_{t_0}^{t_i} (\bar{\bar{\mathbf{X}}}_\theta^a(s) - \bar{\bar{\mathbf{X}}}_\theta^a(t_0)) d\bar{\bar{\mathbf{X}}}_\theta^b(s).$$

The second-order shuffle residual is

$$R_i^{a,b}(\theta) := D_i^a(\theta) D_i^b(\theta) - I_i^{a,b}(\theta) - I_i^{b,a}(\theta).$$

We then define the shuffle loss by

$$\mathcal{L}_{\text{shuffle}}(\theta) := \frac{1}{N} \sum_{t_i \in \pi[0, T]} \sum_{a, b=1}^m \left| R_i^{a, b}(\theta) \right|^2,$$

where $N = |\pi[0, T]|$ is the number of training time points.

The integrals in $I_i^{a, b}(\theta)$ are not computed through signature libraries such as *iisignature* or *signature*, since those libraries return geometric signatures and therefore satisfy the shuffle identities by construction. Instead, we use left-point Riemann sums, so that the non-geometric deviation can be measured directly. More precisely, if

$$t_0 = s_0 < s_1 < \dots < s_{r_i} = t_i$$

is a partition of $[t_0, t_i]$, then

$$I_i^{a, b}(\theta) := \sum_{\ell=1}^{r_i} (\bar{\mathbf{X}}_{\theta}^a(s_{\ell-1}) - \bar{\mathbf{X}}_{\theta}^a(s_0)) (\bar{\mathbf{X}}_{\theta}^b(s_{\ell}) - \bar{\mathbf{X}}_{\theta}^b(s_{\ell-1})).$$

Definition 3.8 (Physics-informed loss). The physics-informed loss is used to fit the observed path values along the training partition. For each $t_i \in \pi[0, T]$, we first compute the truncated signature of the learned extended path $\bar{\mathbf{X}}_{\theta}$ over $[0, t_i]$, and then pass it through a predictor g_{ϕ} . The loss is defined by

$$\mathcal{L}_{\text{phy}}(\theta, \phi) := \frac{1}{N} \sum_{t_i \in \pi[0, T]} \left\| \mathbf{Y}_{t_i} - g_{\phi}(\mathbf{Sig}^k(\bar{\mathbf{X}}_{\theta})_{0t_i}) \right\|^2.$$

Here $\pi[0, T]$ is a partition of the time interval, $N = |\pi[0, T]|$ is the number of training time points, $\mathbf{Sig}^k(\bar{\mathbf{X}}_{\theta})_{0t_i}$ denotes the signature of the learned extended path truncated at level k , and g_{ϕ} is a trainable predictor, for example a linear layer or a small neural network.

Remark 3.9. This is the most general form of the loss. For the problems of interest in the subsequent sections, we will define the physics-informed loss in different ways, depending on the nature of the problem. However, the shuffle loss will remain the same throughout.

4. BRANCHED SIGNATURE KERNEL SOLVER FOR ODES

In this section, we develop a branched signature-kernel solver based on a single observed time series in \mathbb{R}^d —in the numerical experiments below, this corresponds to the forcing term f sampled at $N + 1$ points on $[0, T]$. From this single observation we generate $N + 1$ training paths by the count-sampling construction of Definition 2.23, which serves as the foundation for the kernel-based solver developed in the remainder of the section.

4.1. Linear systems of differential equations. Fix matrices $A_0, A_1, \dots, A_m \in \mathbb{R}^{d \times d}$ with A_m invertible, and define the linear operator \mathcal{L} acting on $C^m([0, T], \mathbb{R}^d)$ by

$$\mathcal{L}\mathbf{u}(t) := \sum_{r=0}^m A_r \mathbf{u}^{(r)}(t).$$

The boundary operator \mathcal{B} collects the first m derivatives at $t = 0$:

$$\mathcal{B}\mathbf{u} := (\mathbf{u}(0), \mathbf{u}'(0), \dots, \mathbf{u}^{(m-1)}(0)) = (\mathbf{g}_0, \mathbf{g}_1, \dots, \mathbf{g}_{m-1}) \in \mathbb{R}^{md}, \quad \mathbf{g}_p \in \mathbb{R}^d.$$

Definition 4.1 (Linear ODE system).

$$\begin{cases} \mathcal{L}\mathbf{u}(t) = f(t), & t \in [0, T], \\ \mathcal{B}\mathbf{u} = \mathbf{g}, \end{cases}$$

for unknown $\mathbf{u} : [0, T] \rightarrow \mathbb{R}^d$, forcing $f : [0, T] \rightarrow \mathbb{R}^d$, and initial data $\mathbf{g} = (\mathbf{g}_0, \dots, \mathbf{g}_{m-1}) \in \mathbb{R}^{md}$.

The scalar case $d = 1$ recovers the single-equation form with constants $k_r := A_r \in \mathbb{R}$, and is our running example throughout the section.

4.2. Linear integral method I. Let $\mathbf{K}_{\text{BSig}}^N(\cdot, \cdot)$ be the branched signature kernel truncated at order N defined in the previous section. We now construct an ODE solver based on this kernel (with the geometric signature kernel recovered as a special case) from a single trajectory observation of the forcing f . To our knowledge, this single-trajectory construction is new in the literature.

Count-sampled training paths. Let $0 = t_0 < t_1 < \dots < t_N = T$ be the observation times. By count-sampling (Definition 2.23), the single observation of f generates the $N + 1$ training paths

$$\mathbf{f}_i := (f(t_0), f(t_1), \dots, f(t_i)) \in (\mathbb{R}^d)^{i+1}, \quad i = 0, 1, \dots, N.$$

For any query time $t \in [0, T]$ we write $\mathbf{f}(t) := (f(t_0), \dots, f(t_{j(t)}))$ with $j(t) := \max\{j : t_j \leq t\}$, so that $\mathbf{f}(t_j) = \mathbf{f}_j$.

Componentwise kernel ansatz. We place the ansatz on the highest-order derivative $\mathbf{u}^{(m)}$: for each coordinate $q = 1, \dots, d$,

$$u_q^{(m)}(t) = \sum_{i=0}^N \alpha_i^{(q)} \mathbf{K}_{\text{BSig}}^N(\mathbf{f}_i, \mathbf{f}(t)), \quad q = 1, \dots, d. \quad (4.1)$$

Stacking the coordinate coefficients into $\boldsymbol{\alpha}_i := (\alpha_i^{(1)}, \dots, \alpha_i^{(d)})^\top \in \mathbb{R}^d$, the ansatz reads in vector form

$$\mathbf{u}^{(m)}(t) = \sum_{i=0}^N \boldsymbol{\alpha}_i \mathbf{K}_{\text{BSig}}^N(\mathbf{f}_i, \mathbf{f}(t)). \quad (4.2)$$

Successive integration of (4.2) together with the boundary data $\mathcal{B}\mathbf{u} = \mathbf{g}$ gives, for $k = 1, \dots, m$,

$$\mathbf{u}^{(m-k)}(t) = \sum_{i=0}^N \boldsymbol{\alpha}_i (\mathcal{I}^k \mathbf{K}_{\text{BSig}}^N)(\mathbf{f}_i, \mathbf{f}(t)) + \mathbf{p}_{k-1}(t), \quad (4.3)$$

where \mathcal{I}^k is k -fold integration of the kernel in its second argument,

$$(\mathcal{I}^k \mathbf{K}_{\text{BSig}}^N)(\mathbf{f}_i, \mathbf{f}(t)) := \int_0^t \int_0^{s_1} \dots \int_0^{s_{k-1}} \mathbf{K}_{\text{BSig}}^N(\mathbf{f}_i, \mathbf{f}(s_k)) ds_k \dots ds_1,$$

and $\mathbf{p}_{k-1}(t) \in \mathbb{R}^d$ is the degree- $(k-1)$ Taylor polynomial fixed by the prescribed initial conditions,

$$\mathbf{p}_{k-1}(t) = \sum_{l=0}^{k-1} \frac{t^l}{l!} \mathbf{g}_{m-k+l}.$$

With the convention $\mathcal{I}^0 \mathbf{K}_{\text{BSig}}^N = \mathbf{K}_{\text{BSig}}^N$ and $\mathbf{p}_{-1} \equiv 0$, formula (4.3) is also valid for $k = 0$ and recovers (4.2). In particular, $k = m$ yields $\mathbf{u}(t)$ itself.

Collocation block system. Applying \mathcal{L} to the ansatz via (4.3),

$$\mathcal{L}\mathbf{u}(t) = \sum_{i=0}^N \left[\sum_{r=0}^m A_r (\mathcal{I}^{m-r} \mathbf{K}_{\text{BSig}}^N)(\mathbf{f}_i, \mathbf{f}(t)) \right] \boldsymbol{\alpha}_i + \sum_{r=0}^{m-1} A_r \mathbf{p}_{m-r-1}(t),$$

and collocating $\mathcal{L}\mathbf{u}(t_j) = \mathbf{f}(t_j)$ at every count-sampled path $j = 0, \dots, N$ yields the block linear system

$$\sum_{i=0}^N L_{ji} \boldsymbol{\alpha}_i = \tilde{\mathbf{f}}(t_j), \quad j = 0, \dots, N, \quad (4.4)$$

with $d \times d$ blocks

$$L_{ji} := \sum_{r=0}^m A_r (\mathcal{I}^{m-r} \mathbf{K}_{\text{BSig}}^N)(\mathbf{f}_i, \mathbf{f}_j) \in \mathbb{R}^{d \times d}, \quad (4.5)$$

and reduced forcing $\tilde{\mathbf{f}}(t_j) := \mathbf{f}(t_j) - \sum_{r=0}^{m-1} A_r \mathbf{p}_{m-r-1}(t_j) \in \mathbb{R}^d$. Equivalently, in matrix form,

$$L \boldsymbol{\alpha} = \tilde{\mathbf{F}}, \quad L \in \mathbb{R}^{(N+1)d \times (N+1)d}, \quad \boldsymbol{\alpha} = (\boldsymbol{\alpha}_0^\top, \dots, \boldsymbol{\alpha}_N^\top)^\top, \quad \tilde{\mathbf{F}} = (\tilde{\mathbf{f}}(t_0)^\top, \dots, \tilde{\mathbf{f}}(t_N)^\top)^\top.$$

Boundary constraints. Evaluating the integrated ansatz (4.3) at $t = 0$ and using $\mathbf{p}_{k-1}(0) = \mathbf{g}_{m-k}$ gives, for $p = 0, \dots, m-1$,

$$\mathbf{u}^{(p)}(0) = \sum_{i=0}^N \alpha_i (\mathcal{I}^{m-p} \mathbf{K}_{\text{BSig}}^N)(\mathbf{f}_i, \mathbf{f}_0) \Big|_{t=0} + \mathbf{g}_p = \mathbf{g}_p,$$

so that the iterated integrals vanish identically at $t = 0$ and the initial conditions are satisfied by construction through \mathbf{p}_{k-1} . The free boundary constraints that remain are therefore the natural matching relations at the degenerate first path $\mathbf{f}_0 = (f(t_0))$, encoded as the block system

$$B \boldsymbol{\alpha} = \mathbf{g}, \quad B_{p,i} := (\mathcal{I}^{m-p} \mathbf{K}_{\text{BSig}}^N)(\mathbf{f}_i, \mathbf{f}_0) \Big|_{t=t_0} \in \mathbb{R}^{d \times d}, \quad p = 0, \dots, m-1, \quad (4.6)$$

where the evaluation $|_{t=t_0}$ enforces compatibility at the boundary node per Definition 2.23.

Augmented least-squares system. The combined collocation and boundary system

$$\begin{pmatrix} L \\ B \end{pmatrix} \boldsymbol{\alpha} = \begin{pmatrix} \tilde{F} \\ \mathbf{g} \end{pmatrix}$$

has $(N+1)d$ unknowns and $(N+1+m)d$ equations. We close it by the weighted least-squares problem

$$\boldsymbol{\alpha} = \arg \min_{\boldsymbol{\alpha} \in \mathbb{R}^{(N+1)d}} \|L \boldsymbol{\alpha} - \tilde{F}\|^2 + \lambda_B \|B \boldsymbol{\alpha} - \mathbf{g}\|^2, \quad (4.7)$$

with tunable boundary weight $\lambda_B > 0$.

Evaluation within $[0, T]$. Once $\boldsymbol{\alpha}$ has been recovered from (4.7), the solution at a new query time $\tau \in [0, T]$ is obtained by integrating the ansatz m times,

$$\mathbf{u}(\tau) = \sum_{i=0}^N \alpha_i (\mathcal{I}^m \mathbf{K}_{\text{BSig}}^N)(\mathbf{f}_i, \mathbf{f}(\tau)) + \mathbf{p}_{m-1}(\tau), \quad (4.8)$$

where the same count-sampled training paths $\mathbf{f}_0, \dots, \mathbf{f}_N$ act as the kernel anchors.

Example 4.2 (Linear ODE: scalar integral method). *Consider the scalar second-order ODE*

$$\begin{aligned} k_2 u''(t) + k_1 u'(t) + k_0 u(t) &= f(t), & t \in [0, T], \\ u(0) &= a, & u'(0) = b, \end{aligned}$$

with constants $k_0, k_1, k_2 \in \mathbb{R}$ ($k_2 \neq 0$), corresponding to the $d = 1$, $m = 2$ instance of Definition 4.1 with $A_r = k_r$ and initial data $g_0 = a$, $g_1 = b$.

We use Example 4.2 to demonstrate our general solver construction. Following the integral method of Section 4.2, we place the kernel ansatz on the highest-order derivative u'' and recover the lower derivatives and the solution itself by integrating the kernel (not the forcing f):

$$u''(t) = \sum_{i=0}^N \alpha_i \mathbf{K}_{\text{BSig}}^N(\mathbf{f}_i, \mathbf{f}(t)), \quad (4.9)$$

where $\mathbf{f}_0, \dots, \mathbf{f}_N$ are the count-sampled training paths $\mathbf{f}_i = (f(t_0), \dots, f(t_i))$ on the grid $0 = t_0 < t_1 < \dots < t_N = T$.

Following the method derived in Section 4.2, and the initial condition $u'(0) = b$, $u(0) = a$, we get

$$\begin{aligned} u'(t) &= b + \int_0^t u''(s) ds = b + \sum_{i=0}^N \alpha_i (\mathcal{I} \mathbf{K}_{\text{BSig}}^N)(\mathbf{f}_i, \mathbf{f}(t)); \\ u(t) &= a + bt + \int_0^t \int_0^s u''(r) dr ds = a + bt + \sum_{i=0}^N \alpha_i (\mathcal{I}^2 \mathbf{K}_{\text{BSig}}^N)(\mathbf{f}_i, \mathbf{f}(t)). \end{aligned}$$

which then constructs the equation for equation (4.3) with boundary polynomials $\mathbf{p}_0(t) = b$ and $\mathbf{p}_1(t) = a + bt$.

Matrix linear system. Collocating the ODE at $t = t_j$ for $j = 0, \dots, N$ and substituting the three expressions above gives

$$\sum_{i=0}^N \alpha_i \left[k_2 \mathbf{K}_{\text{BSig}}^N(\mathbf{f}_i, \mathbf{f}_j) + k_1 (\mathcal{I} \mathbf{K}_{\text{BSig}}^N)(\mathbf{f}_i, \mathbf{f}_j) + k_0 (\mathcal{I}^2 \mathbf{K}_{\text{BSig}}^N)(\mathbf{f}_i, \mathbf{f}_j) \right] = f(t_j) - k_1 b - k_0 (a + b t_j).$$

Introduce the three $(N+1) \times (N+1)$ Gram matrices

$$K_{ji} := \mathbf{K}_{\text{BSig}}^N(\mathbf{f}_i, \mathbf{f}_j), \quad K_{ji}^{(1)} := (\mathcal{I} \mathbf{K}_{\text{BSig}}^N)(\mathbf{f}_i, \mathbf{f}_j), \quad K_{ji}^{(2)} := (\mathcal{I}^2 \mathbf{K}_{\text{BSig}}^N)(\mathbf{f}_i, \mathbf{f}_j),$$

so that the ansatz values at the collocation nodes are

$$\mathbf{u}''(\mathbf{t}) = K \boldsymbol{\alpha}, \quad \mathbf{u}'(\mathbf{t}) = b \mathbf{1} + K^{(1)} \boldsymbol{\alpha}, \quad \mathbf{u}(\mathbf{t}) = a \mathbf{1} + b \mathbf{t} + K^{(2)} \boldsymbol{\alpha},$$

with $\mathbf{t} = (t_0, \dots, t_N)^\top$, $\boldsymbol{\alpha} = (\alpha_0, \dots, \alpha_N)^\top$, and $\mathbf{1} \in \mathbb{R}^{N+1}$ the all-ones vector. Substituting into the ODE evaluated at \mathbf{t} ,

$$k_2 K \boldsymbol{\alpha} + k_1 (b \mathbf{1} + K^{(1)} \boldsymbol{\alpha}) + k_0 (a \mathbf{1} + b \mathbf{t} + K^{(2)} \boldsymbol{\alpha}) = \mathbf{f}, \quad \mathbf{f} := (f(t_0), \dots, f(t_N))^\top,$$

collecting terms yields the block linear system

$$L \boldsymbol{\alpha} = \tilde{F}, \quad L := k_2 K + k_1 K^{(1)} + k_0 K^{(2)} \in \mathbb{R}^{(N+1) \times (N+1)}, \quad (4.10)$$

with reduced forcing

$$\tilde{F} := \mathbf{f} - (k_0 a + k_1 b) \mathbf{1} - k_0 b \mathbf{t} \in \mathbb{R}^{N+1}.$$

Equation (4.10) is the scalar $m = 2$ specialization of the block kernel system (4.5), with no integration applied to f . We demonstrate this example in Section 6 with a real-world application.

4.3. Linear integral method II. In Section 4.2, we placed the kernel ansatz on the highest-order derivative $\mathbf{u}^{(m)}$ and integrated m times to recover \mathbf{u} . When the forcing term f is very rough, however, the differential method is sensitive to noise in f and inherits its low regularity in every block of L . An equivalent — and numerically preferable — formulation is to integrate *both sides* of the ODE m times first, turning the differential equation into an integral equation in \mathbf{u} itself, and then place the kernel ansatz directly on \mathbf{u} .

We begin with a second-order scalar ODE to demonstrate the main idea. To fix notation, consider the damped oscillator with prescribed parameters (m, c, k) :

$$m u''(t) + c u'(t) + k u(t) = f(t), \quad u(t_0) = u_0, \quad u'(t_0) = v_0.$$

Here $f(t)$ denotes the external forcing signal. Integrating both sides twice from t_0 to t and applying the fundamental theorem of calculus together with the initial conditions yields the Volterra integral equation

$$m u(t) + c \int_{t_0}^t u(s) ds + k \int_{t_0}^t \int_{t_0}^s u(r) dr ds = \int_{t_0}^t \int_{t_0}^s f(r) dr ds + m u_0 + (m v_0 + c u_0)(t - t_0). \quad (4.11)$$

The differential equation has been transformed into an integral equation in u alone, whose right-hand side depends only on the iterated integral of f and on the initial data. No derivatives of u remain on the left.

General order- m , d -dimensional formulation. Apply the m -fold integration operator

$$(\mathcal{I}_{t_0}^m \phi)(t) := \int_{t_0}^t \int_{t_0}^{s_1} \cdots \int_{t_0}^{s_{m-1}} \phi(s_m) ds_m \cdots ds_1$$

to both sides of $\mathcal{L} \mathbf{u}(t) = f(t)$. Repeated use of the fundamental theorem of calculus, together with the initial conditions $\mathbf{u}^{(l)}(t_0) = \mathbf{g}_l$ for $l = 0, \dots, m-1$, gives the identity

$$(\mathcal{I}_{t_0}^m \mathbf{u}^{(r)})(t) = (\mathcal{I}_{t_0}^{m-r} \mathbf{u})(t) - \sum_{l=0}^{r-1} \frac{(t-t_0)^{m-r+l}}{(m-r+l)!} \mathbf{g}_l, \quad r = 0, 1, \dots, m, \quad (4.12)$$

which for $r = m$ reduces to Taylor's theorem with integral remainder and for $r = 0$ is the trivial identity $\mathcal{I}^m \mathbf{u} = \mathcal{I}^m \mathbf{u}$. Summing (4.12) against A_r and rearranging,

$$\sum_{r=0}^m A_r (\mathcal{I}_{t_0}^{m-r} \mathbf{u})(t) = (\mathcal{I}_{t_0}^m f)(t) + \mathbf{q}(t), \quad (4.13)$$

where the boundary polynomial $\mathbf{q}(t) \in \mathbb{R}^d$ collects all initial-conditions,

$$\mathbf{q}(t) := \sum_{r=1}^m A_r \sum_{l=0}^{r-1} \frac{(t-t_0)^{m-r+l}}{(m-r+l)!} \mathbf{g}_l. \quad (4.14)$$

Equation (4.13) is the multi-dimensional, order- m Volterra form of Definition 4.1: all initial conditions $\mathbf{g}_0, \dots, \mathbf{g}_{m-1}$ are absorbed into \mathbf{q} , and only iterated integrals of f and \mathbf{u} appear.

Remark 4.3. For $m = 2$, $d = 1$, with $A_0 = k$, $A_1 = c$, $A_2 = m$, formula (4.14) gives $\mathbf{q}(t) = mu_0 + (mv_0 + cu_0)(t - t_0)$, recovering (4.11).

Kernel ansatz on \mathbf{u} . Because (4.13) contains no derivatives of \mathbf{u} , we place the kernel ansatz directly on the solution: for each coordinate $q = 1, \dots, d$,

$$u_q(t) = \sum_{i=0}^N \alpha_i^{(q)} \mathbf{K}_{\text{BSig}}^N(\mathbf{f}_i, \mathbf{f}(t)), \quad (4.15)$$

or, in vector form with $\boldsymbol{\alpha}_i := (\alpha_i^{(1)}, \dots, \alpha_i^{(d)})^\top \in \mathbb{R}^d$,

$$\mathbf{u}(t) = \sum_{i=0}^N \boldsymbol{\alpha}_i \mathbf{K}_{\text{BSig}}^N(\mathbf{f}_i, \mathbf{f}(t)). \quad (4.16)$$

The count-sampled training paths $\mathbf{f}_0, \dots, \mathbf{f}_N$ defined in Section 4.2 are reused as the kernel anchors.

Substituting (4.16) into (4.13) and collocating at $t = t_j$ for $j = 0, \dots, N$ gives

$$\sum_{i=0}^N L_{ji} \boldsymbol{\alpha}_i = \tilde{\mathbf{f}}_{\text{II}}(t_j), \quad j = 0, \dots, N, \quad (4.17)$$

with the *same* $d \times d$ block kernel matrix as in the differential method (4.5),

$$L_{ji} = \sum_{r=0}^m A_r (\mathcal{I}_{t_0}^{m-r} \mathbf{K}_{\text{BSig}}^N)(\mathbf{f}_i, \mathbf{f}_j) \in \mathbb{R}^{d \times d}, \quad (4.18)$$

and integrated forcing

$$\tilde{\mathbf{f}}_{\text{II}}(t_j) := (\mathcal{I}_{t_0}^m f)(t_j) + \mathbf{q}(t_j) \in \mathbb{R}^d.$$

In the Matrix form, we then have

$$L \boldsymbol{\alpha} = \tilde{\mathbf{F}}_{\text{II}}, \quad \text{with } \tilde{\mathbf{F}}_{\text{II}} = (\tilde{\mathbf{f}}_{\text{II}}(t_0)^\top, \dots, \tilde{\mathbf{f}}_{\text{II}}(t_N)^\top)^\top \in \mathbb{R}^{(N+1)d}. \quad (4.19)$$

4.4. Nonlinear equations. We extend the framework of Section 4.1 to nonlinear systems. Let \mathcal{N} denote a (possibly nonlinear) m -th order differential operator acting on $C^m([0, T], \mathbb{R}^d)$, and recall the boundary operator $\mathcal{B}\mathbf{u} := (\mathbf{u}(0), \mathbf{u}'(0), \dots, \mathbf{u}^{(m-1)}(0))$.

Definition 4.4 (Nonlinear ODE system).

$$\begin{cases} \mathcal{N}\mathbf{u}(t) = f(t), & t \in [0, T], \\ \mathcal{B}\mathbf{u} = \mathbf{g}, \end{cases}$$

for unknown $\mathbf{u} : [0, T] \rightarrow \mathbb{R}^d$, forcing $f : [0, T] \rightarrow \mathbb{R}^d$, and initial data $\mathbf{g} = (\mathbf{g}_0, \dots, \mathbf{g}_{m-1}) \in \mathbb{R}^{md}$. A typical splitting is $\mathcal{N}\mathbf{u} = \mathcal{L}\mathbf{u} + \mathcal{N}_{\text{nl}}(\mathbf{u}, \mathbf{u}', \dots, \mathbf{u}^{(m-1)})$, where \mathcal{L} is the linear operator of Definition 4.1 and \mathcal{N}_{nl} collects the nonlinear contributions.

4.5. Nonlinear integral method. We illustrate the method with the Duffing equation, which serves as one of our main numerical examples, before presenting the general multidimensional formulation.

Definition 4.5 (Duffing equation).

$$\begin{aligned} u''(t) + k_1 u'(t) + k_0 u(t) + \gamma u(t)^3 &= f(t), & t \in [0, T], \\ u(0) = a, & \quad u'(0) = b, \end{aligned}$$

with linear constants $k_0, k_1 \in \mathbb{R}$, nonlinear stiffness $\gamma \in \mathbb{R}$, and initial data $a, b \in \mathbb{R}$. This is the $d = 1$, $m = 2$ instance of Definition 4.4 with linear part $\mathcal{L}u = u'' + k_1 u' + k_0 u$ (so $A_2 = 1$, $A_1 = k_1$, $A_0 = k_0$) and nonlinear part $\mathcal{N}_{\text{nl}}(u) = \gamma u^3$.

Following the integral method of Section 4.3, place the kernel ansatz on u'' and recover the lower derivatives by integrating the kernel:

$$u''(t) = \sum_{i=0}^N \alpha_i \mathbf{K}_{\text{BSig}}^N(\mathbf{f}_i, \mathbf{f}(t)), \quad (4.20)$$

$$u'(t) = b + \sum_{i=0}^N \alpha_i (\mathcal{I} \mathbf{K}_{\text{BSig}}^N)(\mathbf{f}_i, \mathbf{f}(t)), \quad (4.21)$$

$$u(t) = a + bt + \sum_{i=0}^N \alpha_i (\mathcal{I}^2 \mathbf{K}_{\text{BSig}}^N)(\mathbf{f}_i, \mathbf{f}(t)), \quad (4.22)$$

where $\mathbf{f}_0, \dots, \mathbf{f}_N$ are the count-sampled training paths on the grid $0 = t_0 < t_1 < \dots < t_N = T$ from Section 4.2, and the boundary polynomials b and $a + bt$ are the cases $k = 1, 2$ of (4.3). Plugging (4.20)–(4.22) into Definition 4.5 and grouping the linear and nonlinear contributions,

$$\begin{aligned} & \underbrace{\sum_{i=0}^N \alpha_i \left[\mathbf{K}_{\text{BSig}}^N(\mathbf{f}_i, \mathbf{f}(t)) + k_1 (\mathcal{I} \mathbf{K}_{\text{BSig}}^N)(\mathbf{f}_i, \mathbf{f}(t)) + k_0 (\mathcal{I}^2 \mathbf{K}_{\text{BSig}}^N)(\mathbf{f}_i, \mathbf{f}(t)) \right]}_{\text{linear part}} \\ & + \underbrace{\gamma \left[a + bt + \sum_{i=0}^N \alpha_i (\mathcal{I}^2 \mathbf{K}_{\text{BSig}}^N)(\mathbf{f}_i, \mathbf{f}(t)) \right]^3}_{\text{nonlinear part}} = f(t) - k_1 b - k_0(a + bt). \end{aligned} \quad (4.23)$$

The boundary-data contributions $k_1 b$ and $k_0(a + bt)$ have been moved to the right-hand side, exactly as in the linear case (equation (4.10)). Given the above derivation, we then introduce the three Gram matrices, the time vector, and the unit vector,

$$\begin{aligned} K_{ji} &:= \mathbf{K}_{\text{BSig}}^N(\mathbf{f}_i, \mathbf{f}_j), & K_{ji}^{(1)} &:= (\mathcal{I} \mathbf{K}_{\text{BSig}}^N)(\mathbf{f}_i, \mathbf{f}_j), \\ K_{ji}^{(2)} &:= (\mathcal{I}^2 \mathbf{K}_{\text{BSig}}^N)(\mathbf{f}_i, \mathbf{f}_j), & \mathbf{t} &:= (t_0, \dots, t_N)^\top, & \mathbf{1} &\in \mathbb{R}^{N+1}, \end{aligned}$$

so that, at $t = \mathbf{t}$,

$$u''(\mathbf{t}) = K \boldsymbol{\alpha}, \quad u'(\mathbf{t}) = b \mathbf{1} + K^{(1)} \boldsymbol{\alpha}, \quad u(\mathbf{t}) = a \mathbf{1} + b \mathbf{t} + K^{(2)} \boldsymbol{\alpha}.$$

Substituting into the Duffing equation evaluated at \mathbf{t} gives the nonlinear residual equation

$$L \boldsymbol{\alpha} + \gamma (a \mathbf{1} + b \mathbf{t} + K^{(2)} \boldsymbol{\alpha})^{\text{O}3} = \tilde{F}, \quad (4.24)$$

with linear block matrix

$$L := K + k_1 K^{(1)} + k_0 K^{(2)} \in \mathbb{R}^{(N+1) \times (N+1)},$$

reduced forcing

$$\tilde{F} := \mathbf{f} - (k_0 a + k_1 b) \mathbf{1} - k_0 b \mathbf{t} \in \mathbb{R}^{N+1}, \quad \mathbf{f} = (f(t_0), \dots, f(t_N))^\top,$$

and $(\cdot)^{\circ 3}$ denoting the elementwise cube of a vector. Equation (4.24) reduces to the linear block system (4.10) when $\gamma = 0$.

Nonlinear solver. Define the residual map

$$\mathcal{R}(\boldsymbol{\alpha}) := L\boldsymbol{\alpha} + \gamma(a\mathbf{1} + b\mathbf{t} + K^{(2)}\boldsymbol{\alpha})^{\circ 3} - \tilde{F},$$

and the training loss

$$\text{Loss}_{\text{ODE}}(\boldsymbol{\alpha}) := \frac{1}{N+1} \|\mathcal{R}(\boldsymbol{\alpha})\|_2^2.$$

Because \mathcal{R} is a smooth (cubic) polynomial in $\boldsymbol{\alpha}$, we recover the optimal weights via a quasi-Newton scheme:

$$\boldsymbol{\alpha}^* = \underset{\boldsymbol{\alpha} \in \mathbb{R}^{N+1}}{\text{argmin}} \text{Loss}_{\text{ODE}}(\boldsymbol{\alpha}),$$

solved with L-BFGS. Tikhonov regularization $+\lambda \|\boldsymbol{\alpha}\|_2^2$ may be added to the loss for stability.

Evaluation within $[0, T]$. Once $\boldsymbol{\alpha}^*$ has been recovered, the solution and its derivatives at a new query time $\tau \in [0, T]$ are read off from the ansatz (4.20)–(4.22) directly,

$$u''(\tau) = \sum_{i=0}^N \alpha_i^* \mathbf{K}_{\text{BSig}}^N(\mathbf{f}_i, \mathbf{f}(\tau)), \quad u'(\tau) = b + \sum_{i=0}^N \alpha_i^* (\mathcal{I}\mathbf{K}_{\text{BSig}}^N)(\mathbf{f}_i, \mathbf{f}(\tau)),$$

$$u(\tau) = a + b\tau + \sum_{i=0}^N \alpha_i^* (\mathcal{I}^2\mathbf{K}_{\text{BSig}}^N)(\mathbf{f}_i, \mathbf{f}(\tau)).$$

General nonlinear systems. For a general operator $\mathcal{N}\mathbf{u} = \mathcal{L}\mathbf{u} + \mathcal{N}_{\text{nl}}(\mathbf{u}, \mathbf{u}', \dots, \mathbf{u}^{(m-1)})$ with $\mathbf{u} : [0, T] \rightarrow \mathbb{R}^d$, the same recipe yields the multi-dimensional nonlinear residual

$$\mathcal{R}(\boldsymbol{\alpha}) = L\boldsymbol{\alpha} + \Phi_{\text{nl}}(K^{(0)}\boldsymbol{\alpha}, K^{(1)}\boldsymbol{\alpha}, \dots, K^{(m-1)}\boldsymbol{\alpha}; \mathbf{p}_{m-1}, \dots, \mathbf{p}_0) - \tilde{F},$$

where L is the linear block-kernel matrix of (4.5), Φ_{nl} encodes the nodewise evaluation of \mathcal{N}_{nl} at the integrated-kernel reconstructions of $\mathbf{u}, \mathbf{u}', \dots, \mathbf{u}^{(m-1)}$, and the Taylor polynomials \mathbf{p}_{k-1} account for the initial data. The minimization is again carried out by L-BFGS in the $(N+1)d$ unknowns $\boldsymbol{\alpha} = (\boldsymbol{\alpha}_0^\top, \dots, \boldsymbol{\alpha}_N^\top)^\top$.

Remark 4.6. The nonlinear example in this section and its solution are constructed using the method from Section 4.2; in particular, we do not directly integrate (4.23) on the right-hand side.

5. TEST/TRAIN AND RETRAIN METHOD

Building on the branched signature kernel solvers introduced in Section 4, we now describe a streaming protocol for the same ODE problem when only a single trajectory observation of the forcing signal $f(t)$, $t \geq 0$, is available. Suppose that the forcing signal is observed in real time as

$$f(t_0), f(t_1), \dots, f(t_n), f(t_{n+1}), \dots$$

The solvers in Sections 4.2–4.3 fit a single batch of coefficients $\boldsymbol{\alpha} \in \mathbb{R}^{N+1}$ on a fixed observation window $\{t_0, \dots, t_N\}$. Refitting the entire batch whenever a new sample $f(t_{n+1})$ arrives is computationally wasteful. We therefore propose a streaming update scheme in which we (i) train an initial batch model on the first $n+1$ observations, (ii) update the coefficient vector by adding one new entry for each incoming observation, using a closed-form update in the linear case and a scalar Newton step in the nonlinear case, and (iii) periodically retrain the model to control the accumulated signal. We describe the test/train and retraining procedures below, following the branched signature kernel solver developed in Section 4.2. The same procedure can be applied directly to the solvers developed in Section 4.3, and is therefore omitted here.

5.1. Initial training. Let $\mathbf{f}_0, \dots, \mathbf{f}_n$ be the count-sampled training paths from the first $n + 1$ observations, $\mathbf{f}_i = (f(t_0), \dots, f(t_i))$, and let $\mathbf{t}^{(n)} = (t_0, \dots, t_n)^\top$, $\mathbf{f}^{(n)} = (f(t_0)^\top, \dots, f(t_n)^\top)^\top \in \mathbb{R}^{(n+1)d}$.

For the linear ODE system of Definition 4.1 with operator $\mathcal{L} = \sum_{r=0}^m A_r d^r/dt^r$, the batch collocation system of Section 4.2 is

$$L_n \boldsymbol{\alpha}^{(n)} = \tilde{\mathbf{F}}^{(n)}, \quad (5.1)$$

with block matrix and reduced forcing

$$L_n := \sum_{r=0}^m A_r \otimes K^{(m-r)} \in \mathbb{R}^{(n+1)d \times (n+1)d}, \quad \tilde{\mathbf{F}}^{(n)} := \mathbf{f}^{(n)} - \sum_{r=0}^{m-1} (I_{n+1} \otimes A_r) \mathbf{P}_{m-r-1}^{(n)}.$$

Here the scalar Gram matrices have entries $K_{ji}^{(k)} = (\mathcal{I}^k \mathbf{K}_{\text{BSig}}^N)(\mathbf{f}_i, \mathbf{f}_j)$ for $0 \leq i, j \leq n$ and $k = 0, 1, \dots, m$ (with the convention $\mathcal{I}^0 \mathbf{K}_{\text{BSig}}^N = \mathbf{K}_{\text{BSig}}^N$), $A_r \otimes K^{(m-r)}$ denotes the Kronecker product placing the $d \times d$ block A_r into each (j, i) position weighted by $K_{ji}^{(m-r)}$, and $\mathbf{P}_k^{(n)} \in \mathbb{R}^{(n+1)d}$ stacks the Taylor polynomials $\mathbf{p}_k(t_j) = \sum_{l=0}^k \frac{t_j^l}{l!} \mathbf{g}_{m-k-1+l}$ at the observation times,

$$\mathbf{P}_k^{(n)} := (\mathbf{p}_k(t_0)^\top, \dots, \mathbf{p}_k(t_n)^\top)^\top.$$

Solve (5.1) for $\boldsymbol{\alpha}^{(n)} = (\boldsymbol{\alpha}_0^\top, \dots, \boldsymbol{\alpha}_n^\top)^\top \in \mathbb{R}^{(n+1)d}$ directly, or via Tikhonov-regularized least squares.

5.2. Online update. When the next observation $f(t_{n+1}) \in \mathbb{R}^d$ arrives, the collocation system grows to size $(n+2)d \times (n+2)d$. Let L_{n+1} and $\tilde{\mathbf{F}}^{(n+1)}$ denote the augmented block matrix and forcing. Rather than refit all $n+2$ block-coefficients, we *freeze* the previously computed $\boldsymbol{\alpha}_0, \dots, \boldsymbol{\alpha}_n$ and solve only for the new d -dimensional entry $\boldsymbol{\alpha}_{n+1} \in \mathbb{R}^d$ from the new block-collocation row:

$$\sum_{k=0}^{n+1} \Phi_{n+1,k} \boldsymbol{\alpha}_k = \tilde{\mathbf{f}}^{(n+1)}(t_{n+1}),$$

where each $d \times d$ block

$$\Phi_{j,i} := \sum_{r=0}^m A_r (\mathcal{I}^{m-r} \mathbf{K}_{\text{BSig}}^N)(\mathbf{f}_i, \mathbf{f}_j)$$

is the (j, i) entry of the block matrix L_n extended to index $n+1$, and

$$\tilde{\mathbf{f}}^{(n+1)}(t_{n+1}) := f(t_{n+1}) - \sum_{r=0}^{m-1} A_r \mathbf{p}_{m-r-1}(t_{n+1}).$$

Isolating $\boldsymbol{\alpha}_{n+1}$ gives the closed-form update

$$\hat{\boldsymbol{\alpha}}_{n+1} = \Phi_{n+1,n+1}^{-1} \left[\tilde{\mathbf{f}}^{(n+1)}(t_{n+1}) - \sum_{k=0}^n \Phi_{n+1,k} \boldsymbol{\alpha}_k \right]. \quad (5.2)$$

The diagonal block $\Phi_{n+1,n+1} = \sum_{r=0}^m A_r (\mathcal{I}^{m-r} \mathbf{K}_{\text{BSig}}^N)(\mathbf{f}_{n+1}, \mathbf{f}_{n+1})$ is invertible whenever A_m is invertible and the time step is positive (the iterated integrals $\mathcal{I}^k \mathbf{K}_{\text{BSig}}^N$ contribute scalar weights that decay with k , so the leading A_m term dominates for non-degenerate $t_{n+1} > t_n$).

The solution at the new node follows from the prediction formula (4.8),

$$\mathbf{u}(t_{n+1}) = \mathbf{p}_{m-1}(t_{n+1}) + \sum_{k=0}^n \boldsymbol{\alpha}_k (\mathcal{I}^m \mathbf{K}_{\text{BSig}}^N)(\mathbf{f}_k, \mathbf{f}_{n+1}) + \hat{\boldsymbol{\alpha}}_{n+1} (\mathcal{I}^m \mathbf{K}_{\text{BSig}}^N)(\mathbf{f}_{n+1}, \mathbf{f}_{n+1}).$$

By induction, (5.2) produces $\hat{\boldsymbol{\alpha}}_{n+2}, \hat{\boldsymbol{\alpha}}_{n+3}, \dots$ using only previously fitted weights. Each online step costs $O(nd^2)$ to assemble the new kernel block-row plus $O(d^3)$ to invert $\Phi_{n+1,n+1}$, versus $O((nd)^3)$ for a full refit.

The frozen-coefficient update is exact in $\boldsymbol{\alpha}_{n+1}$ given the old coefficients, but is *not* equivalent to the full batch least-squares solution on $n+2$ samples — in which all $\boldsymbol{\alpha}_0, \dots, \boldsymbol{\alpha}_{n+1}$ would shift

jointly. The error introduced by holding the old coefficients fixed accumulates with each streaming step, motivating the retraining schedule below.

5.3. Periodic retraining. Empirically the frozen-coefficient update yields accurate predictions for roughly 10–20 streaming steps before drift becomes visible. Past that horizon we restore accuracy by refitting the full batch on the most recent window $\{\mathbf{f}_{j-n_0}, \dots, \mathbf{f}_j\}$, where n_0 is a fixed look-back size. Letting $\kappa \in \{10, \dots, 20\}$ be the retraining cadence, the complete streaming protocol is:

Algorithm (linear case). *Input:* initial block size n_0 , cadence κ . Compute $\boldsymbol{\alpha}^{(n_0)}$ by solving (5.1) on $\{\mathbf{f}_0, \dots, \mathbf{f}_{n_0}\}$. For $j = n_0 + 1, n_0 + 2, \dots$: (i) if $(j - n_0) \bmod \kappa \neq 0$, apply (5.2) to obtain $\hat{\boldsymbol{\alpha}}_j$; (ii) otherwise, refit the full block on the sliding window $\{\mathbf{f}_{j-n_0}, \dots, \mathbf{f}_j\}$ to obtain a fresh $\boldsymbol{\alpha}^{(j)}$, then resume online updates from index j .

5.4. Nonlinear case. For the nonlinear ODE system of Definition 4.4 with operator $\mathcal{N}\mathbf{u} = \mathcal{L}\mathbf{u} + \mathcal{N}_{\text{nl}}(\mathbf{u}, \mathbf{u}', \dots, \mathbf{u}^{(m-1)})$, the batch collocation residual from Section 4.5 is

$$\mathcal{R}(\boldsymbol{\alpha}^{(n)}) = L_n \boldsymbol{\alpha}^{(n)} + \Phi_{\text{nl}}(\boldsymbol{\alpha}^{(n)}) - \tilde{F}^{(n)},$$

where $\Phi_{\text{nl}}(\boldsymbol{\alpha}^{(n)}) \in \mathbb{R}^{(n+1)d}$ stacks the componentwise nonlinear contributions $\mathcal{N}_{\text{nl}}(\mathbf{u}(t_j), \mathbf{u}'(t_j), \dots, \mathbf{u}^{(m-1)}(t_j))$ evaluated via the integrated-kernel reconstructions $\mathbf{u}^{(r)}(t_j) = \mathbf{p}_{m-r-1}(t_j) + \sum_{k=0}^n \alpha_k (\mathcal{I}^{m-r} \mathbf{K}_{\text{BSig}}^N)(\mathbf{f}_k, \mathbf{f}_j)$ for $r = 0, \dots, m-1$. Initial training minimizes $\|\mathcal{R}\|_2^2 + \lambda \|\boldsymbol{\alpha}\|_2^2$ by L-BFGS.

Online Newton update. When $f(t_{n+1})$ arrives, freeze $\boldsymbol{\alpha}_0, \dots, \boldsymbol{\alpha}_n$ and solve for the new block $\boldsymbol{\alpha}_{n+1} \in \mathbb{R}^d$. Define the previous-coefficient contributions at the new node and the diagonal self-kernel scalars,

$$\mathbf{u}_{\text{prev}}^{(r)}(t_{n+1}) := \mathbf{p}_{m-r-1}(t_{n+1}) + \sum_{k=0}^n \alpha_k (\mathcal{I}^{m-r} \mathbf{K}_{\text{BSig}}^N)(\mathbf{f}_k, \mathbf{f}_{n+1}), \quad \kappa_r := (\mathcal{I}^{m-r} \mathbf{K}_{\text{BSig}}^N)(\mathbf{f}_{n+1}, \mathbf{f}_{n+1}),$$

for $r = 0, 1, \dots, m$. The full ansatz values at t_{n+1} are

$$\mathbf{u}^{(r)}(t_{n+1}) = \mathbf{u}_{\text{prev}}^{(r)}(t_{n+1}) + \kappa_r \boldsymbol{\alpha}_{n+1}.$$

Substituting the freeze-and-solve decomposition $\mathbf{u}^{(r)}(t_{n+1}) = \mathbf{u}_{\text{prev}}^{(r)}(t_{n+1}) + \kappa_r \boldsymbol{\alpha}_{n+1}$ into $\mathcal{N}\mathbf{u}(t_{n+1}) = f(t_{n+1})$ and separating the $\boldsymbol{\alpha}_{n+1}$ -dependent terms from the previous-coefficient terms yields, for $\mathcal{N}\mathbf{u} = \mathcal{L}\mathbf{u} + \mathcal{N}_{\text{nl}}$,

$$\sum_{r=0}^m A_r \mathbf{u}^{(r)}(t_{n+1}) = \Phi_{n+1, n+1} \boldsymbol{\alpha}_{n+1} + \mathbf{c}_0, \quad \Phi_{n+1, n+1} := \sum_{r=0}^m A_r \kappa_r, \quad \mathbf{c}_0 := \sum_{r=0}^m A_r \mathbf{u}_{\text{prev}}^{(r)}(t_{n+1}).$$

Subtracting $f(t_{n+1})$ from both sides gives the d -dimensional nonlinear residual equation in $\boldsymbol{\alpha}_{n+1} \in \mathbb{R}^d$,

$$\begin{aligned} & \mathbf{g}(\boldsymbol{\alpha}_{n+1}) \\ & := \Phi_{n+1, n+1} \boldsymbol{\alpha}_{n+1} + \mathbf{c}_0 + \mathcal{N}_{\text{nl}}\left(\mathbf{u}_{\text{prev}}^{(0)}(t_{n+1}) + \kappa_0 \boldsymbol{\alpha}_{n+1}, \dots, \mathbf{u}_{\text{prev}}^{(m-1)}(t_{n+1}) + \kappa_{m-1} \boldsymbol{\alpha}_{n+1}\right) - f(t_{n+1}) \\ & = \mathbf{0}. \end{aligned} \tag{5.3}$$

The diagonal block $\Phi_{n+1, n+1} \in \mathbb{R}^{d \times d}$ coincides with the $(n+1, n+1)$ -block of L_{n+1} in (5.2), and the constant $\mathbf{c}_0 \in \mathbb{R}^d$ is the linear operator \mathcal{L} applied to the previous-coefficient reconstructions,

$$\mathbf{c}_0 := \sum_{r=0}^m A_r \mathbf{u}_{\text{prev}}^{(r)}(t_{n+1}) = \sum_{r=0}^m A_r \mathbf{p}_{m-r-1}(t_{n+1}) + \sum_{k=0}^n \Phi_{n+1, k} \alpha_k \in \mathbb{R}^d. \tag{5.4}$$

Setting $\mathcal{N}_{\text{nl}} \equiv 0$ recovers the linear closed-form update (5.2): $\boldsymbol{\alpha}_{n+1} = \Phi_{n+1, n+1}^{-1} (f(t_{n+1}) - \mathbf{c}_0)$.

Solve (5.3) by Newton's method in \mathbb{R}^d ,

$$\boldsymbol{\alpha}_{n+1}^{(s+1)} = \boldsymbol{\alpha}_{n+1}^{(s)} - [\nabla_{\boldsymbol{\alpha}_{n+1}} \mathbf{g}(\boldsymbol{\alpha}_{n+1}^{(s)})]^{-1} \mathbf{g}(\boldsymbol{\alpha}_{n+1}^{(s)}),$$

where the Jacobian is

$$\nabla_{\boldsymbol{\alpha}_{n+1}} \mathbf{g}(\boldsymbol{\alpha}_{n+1}) = \Phi_{n+1,n+1} + \sum_{r=0}^{m-1} \kappa_r \partial_r \mathcal{N}_{\text{nl}}(\mathbf{u}^{(0)}(t_{n+1}), \dots, \mathbf{u}^{(m-1)}(t_{n+1})),$$

and $\partial_r \mathcal{N}_{\text{nl}}$ is the Jacobian of \mathcal{N}_{nl} with respect to its r -th argument. Warm-start from the linear-only solution

$$\boldsymbol{\alpha}_{n+1}^{(0)} = \Phi_{n+1,n+1}^{-1} [f(t_{n+1}) - \mathbf{c}_0],$$

which is the closed-form update (5.2) obtained by setting $\mathcal{N}_{\text{nl}} \equiv 0$. In practice, two to three Newton iterations are sufficient.

Periodic full retraining (Section 5.3) is applied with the same cadence κ , replacing the closed-form linear update by the L-BFGS batch solve from Section 4.5.

Specialization: Duffing equation. For the scalar $d = 1$, $m = 2$ Duffing equation of Definition 4.5 ($u'' + k_1 u' + k_0 u + \gamma u^3 = f$), the nonlinear term is $\mathcal{N}_{\text{nl}}(u) = \gamma u^3$, so (5.3) reduces to the scalar cubic

$$g(\alpha_{n+1}) = \Phi_{n+1,n+1} \alpha_{n+1} + \gamma (u_{\text{prev}}(t_{n+1}) + \kappa_0 \alpha_{n+1})^3 + c_0 - f(t_{n+1}) = 0,$$

where $\Phi_{n+1,n+1} = \kappa_2 + k_1 \kappa_1 + k_0 \kappa_0$, $c_0 = k_1 u_{\text{prev}}^{(1)}(t_{n+1}) + k_0 u_{\text{prev}}^{(0)}(t_{n+1}) + u_{\text{prev}}^{(2)}(t_{n+1})$, and the scalar Newton step uses $g'(\alpha) = \Phi_{n+1,n+1} + 3\gamma \kappa_0 (u_{\text{prev}}(t_{n+1}) + \kappa_0 \alpha)^2$.

Optional kernel choice. For rough or strongly nonlinear forcings, the signature-RBF kernel

$$\mathbf{K}_{\text{BSig}}^{N,\text{RBF}}(\mathbf{f}_i, \mathbf{f}_j) := \exp\left(-\frac{\|S^{(N)}(\mathbf{f}_i) - S^{(N)}(\mathbf{f}_j)\|^2}{2\sigma^2}\right),$$

with $S^{(N)}(\mathbf{f})$ the truncated signature of \mathbf{f} , may be substituted for $\mathbf{K}_{\text{BSig}}^N$ wherever it appears above; all algebraic identities and update formulae carry over unchanged.

Remark 5.1. Our Signature kernel construction is based on the count method, where the count sampling paths have different length, thus the RBF kernel is a type of normalization in our framework.

5.5. Branched model training via a neural network. In the case where we apply the neural network lift to learn the branched extension, we must jointly train to fit both the model and extension. Consider an ODE coupled with a very rough signal $f(t)$. We first construct the time-extended path $\mathbf{f} = (t, f(t))$ and feed it through the network Φ_θ to produce the path extension $\tilde{\mathbf{f}}_\theta$. This extension is then used to compute the shuffle loss

$$\mathcal{L}_{\text{shuffle}}(\theta) := \frac{1}{N} \sum_{t_i \in \pi[0,T]} \sum_{a,b=1}^m \left| R_i^{a,b}(\theta) \right|^2,$$

where

$$R_i^{a,b}(\theta) := D_i^a(\theta) D_i^b(\theta) - I_i^{a,b}(\theta) - I_i^{b,a}(\theta),$$

is the second-order residual. The terms in the residual are defined as

$$D_i^a(\theta) := \tilde{\mathbf{f}}_\theta^a(t_i) - \tilde{\mathbf{f}}_\theta^a(t_0), \quad \text{and} \quad I_i^{a,b}(\theta) := \int_{t_0}^{t_i} (\tilde{\mathbf{f}}_\theta^a(s) - \tilde{\mathbf{f}}_\theta^a(t_0)) d\tilde{\mathbf{f}}_\theta^b(s),$$

for $a, b \in \{1, \dots, m\}$, $t_i \in \pi[0, T]$, and $N = |\pi[0, T]|$, the number of training time points.

The extended path $\tilde{\mathbf{f}}_\theta$ is then formed by the concatenation of the extension onto the original path i.e., $\tilde{\mathbf{f}} := (\mathbf{f}, \tilde{\mathbf{f}}_\theta)$. Next, the Kernel Gram matrices are constructed using a kernel choice and optional normalization. The linear or nonlinear collocation system is then solved using the least squares method or nonlinear L-BFGS method in order to produce the solution coefficients α . This allows us to recover both the solution match and the forcing match from the solution and collocation ansatz. The latter is compared with the true forcing to compute the physics-informed model loss for

a general (non-)linear problem (4.4) with operator $\mathcal{N}\mathbf{u} = \mathcal{L}\mathbf{u} + \mathcal{N}_{\text{nl}}(\mathbf{u}, \mathbf{u}', \dots, \mathbf{u}^{(m-1)})$. The loss is defined as follows.

$$\mathcal{L}_{\text{model}}(\boldsymbol{\alpha}, \theta) := \frac{1}{N+1} \left\| L\boldsymbol{\alpha} + \Phi_{\text{nl}}(K^{(0)}\boldsymbol{\alpha}, K^{(1)}\boldsymbol{\alpha}, \dots, K^{(m-1)}\boldsymbol{\alpha}; \mathbf{p}_{m-1}, \dots, \mathbf{p}_0) - \tilde{F}_\theta \right\|_2^2,$$

where \tilde{F}_θ is the reduced forcing, L is the linear block-kernel matrix of (4.5), Φ_{nl} encodes the node-wise evaluation of \mathcal{N}_{nl} at the integrated-kernel reconstructions of $\mathbf{u}, \mathbf{u}', \dots, \mathbf{u}^{(m-1)}$, and the Taylor polynomials \mathbf{p}_{k-1} account for the initial data. The dependence of the loss on the parameter θ comes from the dependence of extended path on the parameter θ .

We then define two hyperparameters λ_{shuffle} and λ_{model} to place weights on the shuffle loss and model loss respectively. The final model loss is then defined as

$$\mathcal{L}_{\text{total}}(\boldsymbol{\alpha}, \theta) := \lambda_{\text{shuffle}}\mathcal{L}_{\text{shuffle}}(\theta) + \lambda_{\text{model}}\mathcal{L}_{\text{model}}(\boldsymbol{\alpha}, \theta).$$

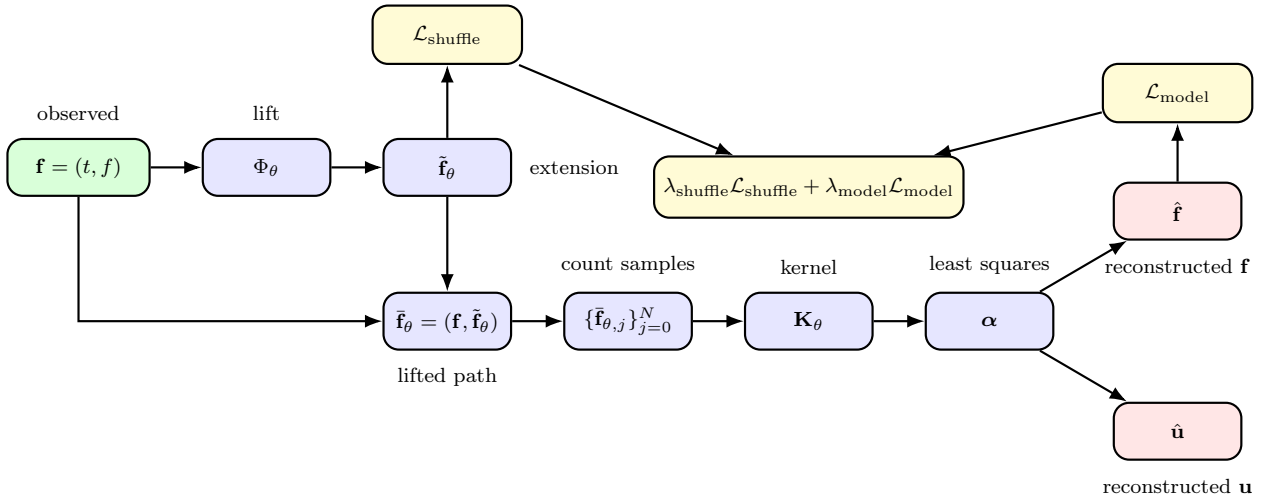


FIGURE 5.1. Neural network lift for branched training architecture of linear ODEs

The parameters λ_{shuffle} and λ_{model} are tuned so that the model learns an extension which fits the data while still following the branched (non-geometric) signature properties. Often, a higher weight is placed on the model loss than the shuffle loss so that a meaningful extension that actually aids in learning the right representative of the solution of the ODE may be selected. In the case of the nonlinear problem, α coefficients from the previous iteration are used as a warm start for the next iteration to improve convergence speed. Illustrative diagram of the linear case is presented in Figure 5.1, while the nonlinear model diagram is shown in Figure 5.2.

5.5.1. A note on Training Landscape. Our joint optimization problem trains a neural network to both learn an extension while fitting the constraints of the differential equation. This is in essence the workflow followed by Physics Informed Neural Networks (PINNs). PINNs are well documented for difficulties within the training process. For example, gradient flows of the different loss components are often imbalanced, leading to optimization imbalances [Wang et al., 2021, Krishnapriyan et al., 2021]. This can be improved through learning rate annealing, network architectures, or gradient normalizations. In our case, specific attention is given to the weighting of shuffle and model loss so that meaningful, nontrivial extensions are learned while sufficient importance is placed on actual model fit. Stiffness and nonlinearity of problems is another essential factor in convergence difficulties [Hao et al., 2025, Wang et al., 2024]. In our cases, we tackle both stiffness and nonlinearity through the use of the RBF signature kernel and tuning of the parameter σ . Tuning this parameter gives better fits for highly stiff, oscillatory problems and greatly increases convergence of the L-BFGS optimizer by improving conditioning. However, overtuning this parameter comes at the risk of overfitting the training, leading to poor performance in out of sample predictions. As of now, both the RBF hyperparameters and loss weightings are tuned to address the issues. In future

work, one may consider methods introduced in the papers above to stabilize convergence for a wider range of problems.

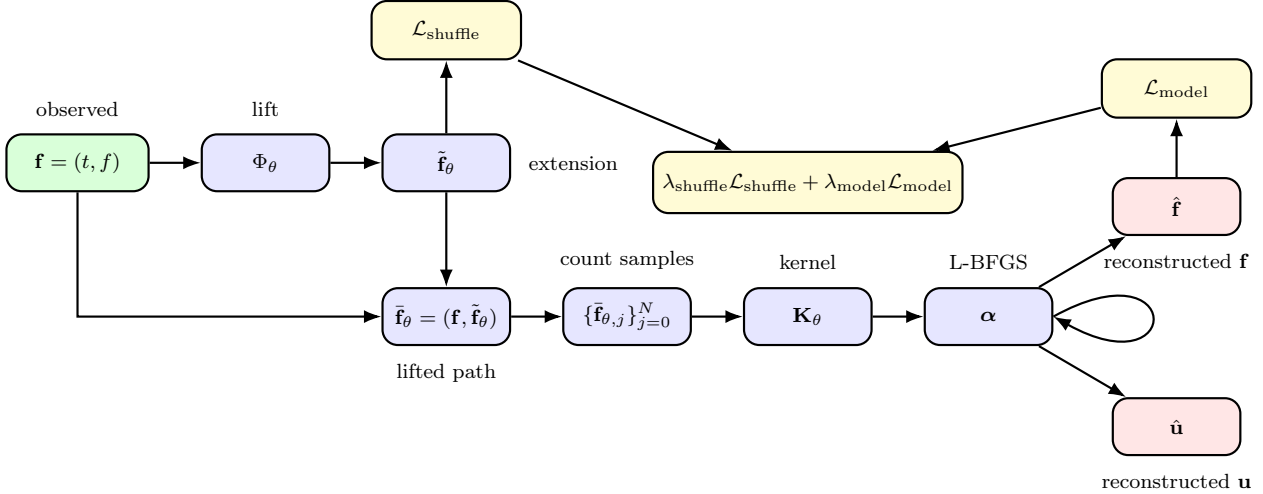


FIGURE 5.2. Neural network lift for branched training architecture of nonlinear ODEs

6. NUMERICAL EXPERIMENTS

We test the branched signature kernel solver developed in Section 4 and Section 5 on a range of examples. In particular, we focus on the setting where only a single trajectory of the forcing term is observed, motivated by real-world scenarios in which the forcing signal is typically noisy. We compare the performance of the geometric signature kernel solver and the branched signature kernel solver when the forcing term is highly rough, such as a sample path of fractional Brownian motion. Branched extensions are constructed in the form of the t -value lift and neural network extension introduced in 3.5 and 3.6. These lift methods are compared to each other and baseline values along with Method 1 and Method 2 in simple examples where the t -value lift captures enough of the branched structure. For more complex problems with rough forcing or nonlinearities, we use the neural network extension to compare calibration and/or testing values against reference solutions.

Across the experiments, we test and consider variations of the truncation level N of the signature, kernel matrix normalization (none or robust) and kernel choices (linear or RBF). We note that within each example, hyper parameters such as regression regularization, L-BFGS tolerance/iteration count, and the RBF sigma value must be tuned correctly. For each section, time lifts are defined by adding a path component of t^α , where $\alpha = 2H$ for the holder value H of the underlying generated forcing. The branched neural network framework consists of a 6 layer MLP with hidden dimensions (512, 256, 128, 64, 32, 16). Model and Shuffle loss, along with iteration count and lambda values are tuned for each problem for convergence. Path extension dimensions are defined within the example problems. All integrations of the Kernel Gram Matrices are done using the cumulative trapezoidal integration method. Ground truth solutions are generated by either high order Runge-Kutta integration or implicit multi-step solvers implemented within the `scipy` library.

6.1. Earthquake displacement model: El-Centro calibration. We apply Method 2 of Section 4.3 to the 1940 El-Centro strong-motion record [Vibrationdata,]. The structural response is modeled by the damped oscillator, which is a special case of Example 4.2:

$$\ddot{u}(t) + 2\xi\omega_n \dot{u}(t) + \omega_n^2 u(t) = -9.81 a(t), \quad u(0) = \dot{u}(0) = 0,$$

where $a(t)$ is the normalized ground-acceleration record, ξ is the damping ratio, and ω_n is the natural frequency.

In the experiment, we take $\xi = 0.02$, $T_n = 5$ s, and $\omega_n = 2\pi/T_n$. We use signature truncation level 12. The signature kernel gram matrix is constructed using the linear signature kernel along with robust normalization on the matrix.

First, calibration is tested along the entire problem interval and displayed in Figure 6.1, which displays fits for both the double integrated forcing and solution approximations. The relative MSE for the double integrated forcing was $1.186030\text{e-}05$ while the relative MSE for the solution was $5.967132\text{e-}06$.

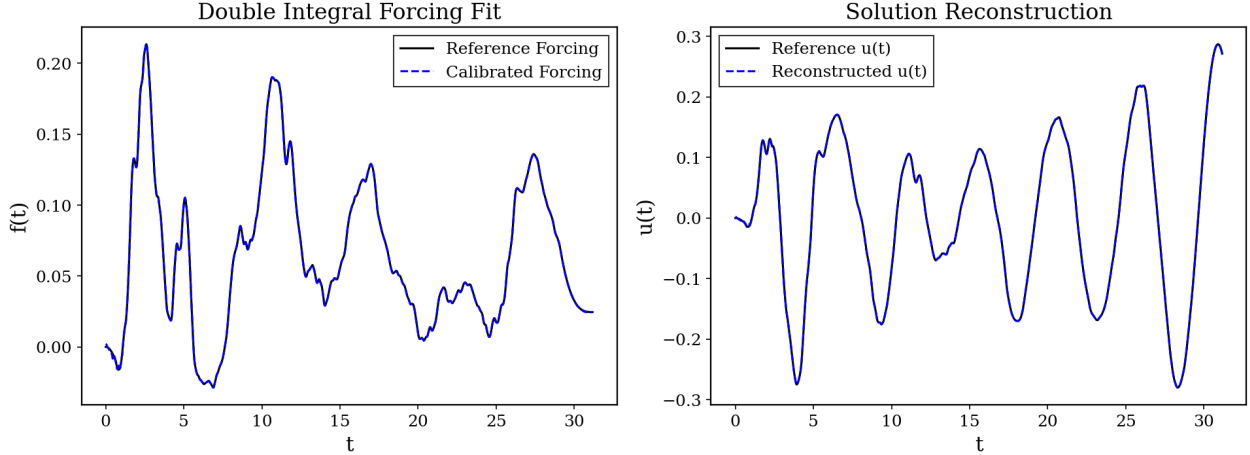


FIGURE 6.1. El-Centro earthquake calibration. Left: forcing calibration-learned kernel representation against $-9.81 a(t)$. Right: displacement-predicted $\hat{u}(t)$ vs. reference $u(t)$.

Next, training and testing were applied using the streaming protocol of Section 5 and the same conditions as the calibration experiment. The initial training window uses the first $n_0 = 200$ observations, and the rolling retrain-and-predict algorithm of Section 5.3 recovers the displacement on the remaining stream. We compare two path constructions for the forcing: the non-branched time-augmented path $(t, -9.81 a(t))$, and the branched augmentation $(t, t^\alpha, -9.81 a(t))$ that adds the time-power channel t^α as a second time coordinate. Through tuning we found the optimal parameter for α to be 0.3, which we used in the experiment. The results for both models are visualized in figure 6.2 and the relative MSE values for training and testing are reported in table 3. The branched model had a 78.30 % improvement in the training forcing and negligible improvement on the training solution. We note that this phenomenon from the solution is likely due to the relatively short training interval, where the initial conditions are enforced well by both models and errors have not yet propagated into the solution. On the testing portion, the branched model had a 99.2% improvement in the forcing and a 61.98% improvement in the solution. From these results, we conclude the branched model outperforms the non-branched model.

TABLE 3. Match results for the Default Kernel model and the t -lift branched model.

	Non Branched model	t -lift branched model	Percent Improvement
Training forcing	9.8437e-13	2.1358e-13	78.3%
Training solution	9.5301e-07	9.5298e-07	0 %
Testing forcing	2.8726e-22	2.3645e-25	99.92 %
Testing solution	3.3817e-02	1.2857e-02	61.98%

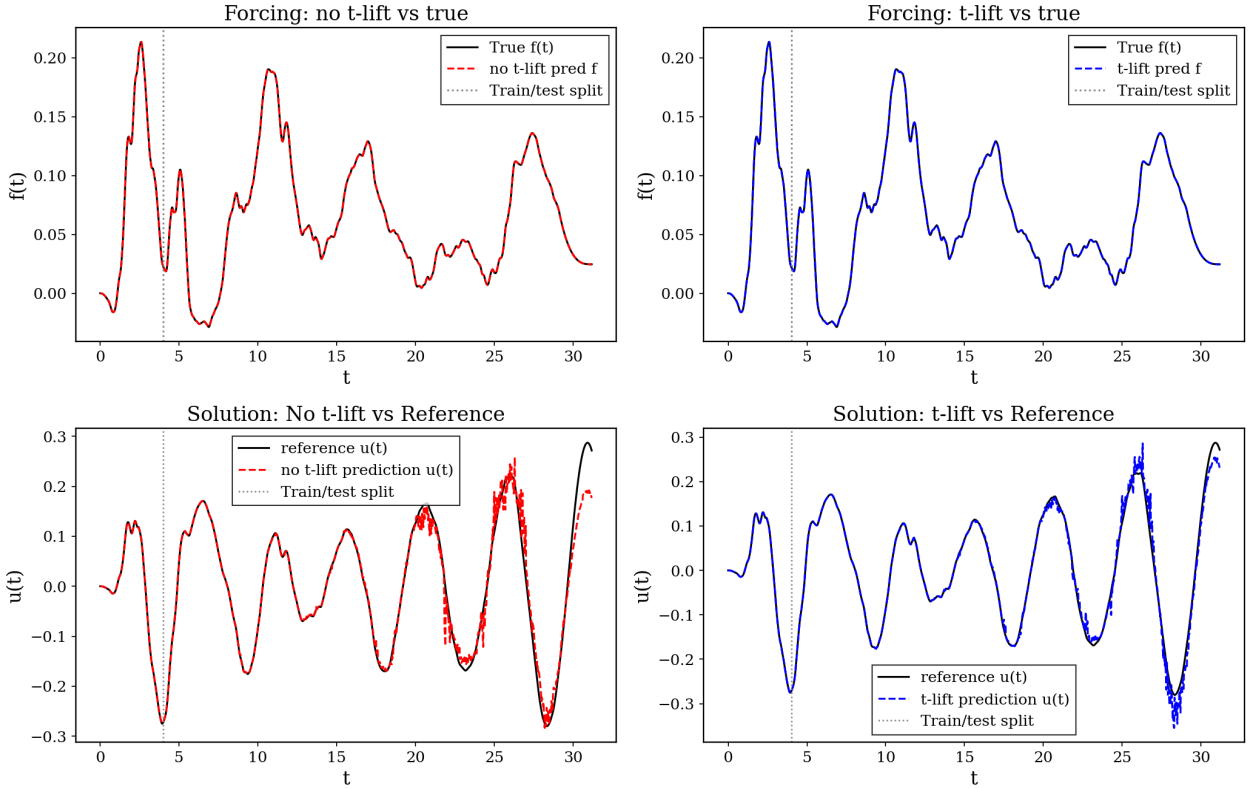


FIGURE 6.2. El-Centro streaming prediction. Top row: forcing calibration; bottom row: solution reconstruction. Left: non-branched path $(t, -9.81 a(t))$. Right: branched path $(t, t^\alpha, -9.81 a(t))$.

6.2. Solow capital-stock model. We apply Method 2 of Section 4.3 to this first order ODE. For this example, we use a modified version of the Solow capital-stock growth model [Solow, 1956], where we use real GDP from FRED [Federal Reserve Bank of St. Louis, 2024] as the forcing term. The Solow capital-stock dynamics are governed by the first-order linear ODE

$$\dot{Y}(t) + \delta Y(t) = s F(t), \quad Y(0) = Y_0,$$

with depreciation rate $\delta \in [0, 1]$, savings rate $s \in [0, 1]$, GDP forcing $F(t)$, and initial capital stock $Y_0 > 0$. In the notation of Definition 4.1, this is the $d = 1$, $m = 1$ instance with $A_1 = 1$, $A_0 = \delta$, forcing $sF(t)$, and initial data $g_0 = Y_0$. In our experiment, we set an initial condition $Y_0 = 3.1$. We apply the linear integral method of Section 4.3 with no normalization and signature truncation level $N = 3$. First consider the results of calibration on the entire interval, shown in figure 6.3. The relative integrated forcing and solution errors were $6.593474e-08$ and $1.186867e-06$ respectively. The lower truncation level here reflects the smooth, first-order nature of the Solow ODE: a depth-3 signature already resolves the dynamics, whereas the second-order El-Centro problem required $N = 12$ for comparable accuracy.

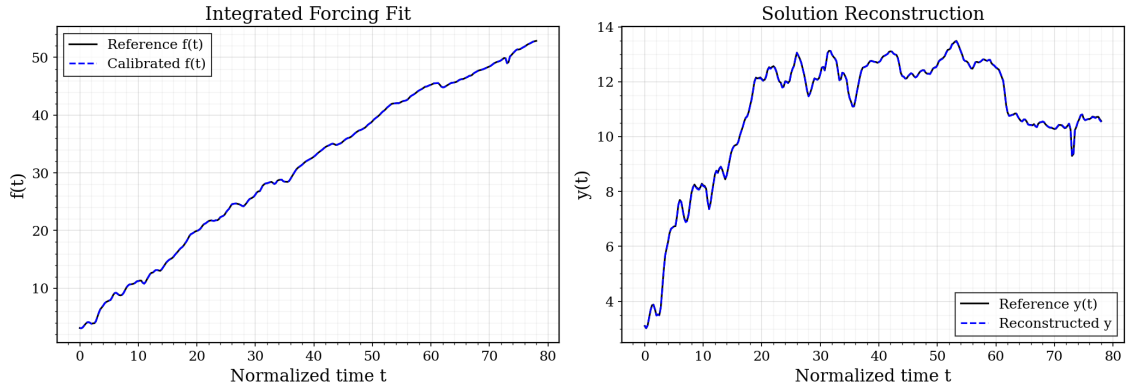


FIGURE 6.3. Solow ODE calibration. Left: GDP forcing match. Right: capital-stock solution match.

Next, a testing and training experiment is done using the rolling retrain protocol of Section 5.3 with initial training window $n_0 = 50$ and retraining cadence $\kappa = 10$ on the non-branched path $(t, F(t))$. This example is well captured through geometric signature kernels with low depth because the GDP data was not rough enough to require a branched extension.

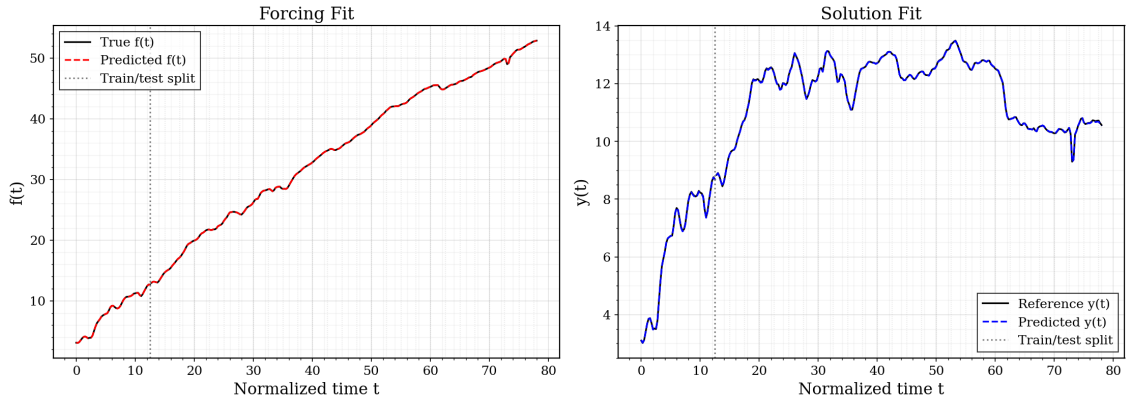


FIGURE 6.4. Solow streaming prediction with the rolling retrain protocol.

TABLE 4. Results

	Non Branched model
Training forcing	1.636290e-06
Training solution	6.187701e-06
Testing forcing	4.763930e-08
Testing solution	8.557833e-07

6.3. Linear ODE with fBM Forcing Example. Consider a linear second order ODE (SDOF equation) driven by a fractional Brownian motion forcing term. We use the following governing equation.

$$m\ddot{U} + c\dot{U} + kU = F(t) \quad U(0) = a, \quad U'(0) = b,$$

We will compare the base signature model to both the t -lift and neural network lift on both training and testing performance. We will also compare methods 1 and 2. For the simulation, $F(t)$ is a 1000 point fBM on the interval from 0 to 1 generated using Davies Harte method with $H = .3$. m, c , and k are set at 1, 5, and 10 respectively. For each method, an RBF signature kernel with $\sigma = 1$ is used. The first 70 percent of values are used for training while the remaining 30 percent are used for testing. Retraining is done every 10 iterations. Robust column normalization was applied and signature depth was fixed to be 3. The neural Network extension dimension was set to be 4.

The results and values of the relative MSE are displayed in the tables below. Table 5 shows the comparisons of both methods and each of the three extension algorithms. Table 6 compares testing and training values for the three extension methods using Method 1, while 7 shows the values for method 2. From the results, it is obvious that method 1 performs the best in all cases. Furthermore, the branched lift outperforms both the baseline model and the t-lift using method 1. This shows it is able to encode the branched information within the paths that the classical signature model fails to pick up. This effect is illustrated in figure 6.5. These results are consistent with method 2 as well with the exception of the predicted integrated forcing. Both this failure and the under-performance of method 2 overall is due to the higher complexity needed in parameter tuning and training for method 2. The integration of the forcing acts as somewhat of a smoother for the data, so the calibration is not able to fit the data as well. For this reason, we recommend using method 1 for problems with nonlinearities, stiffness, or low hurst parameters that provide challenges for parameter tuning and calibration convergence. The training and testing results of our best model, the branched neural network lift using method 1, are presented in 6.6.

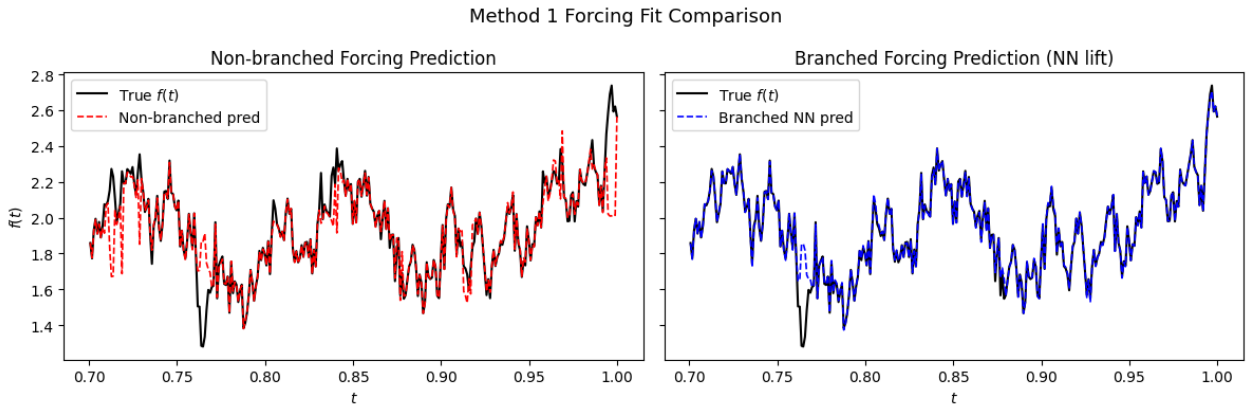


FIGURE 6.5. Predicted Forcing for the normal signature vs branched signature model for Problem 6.3

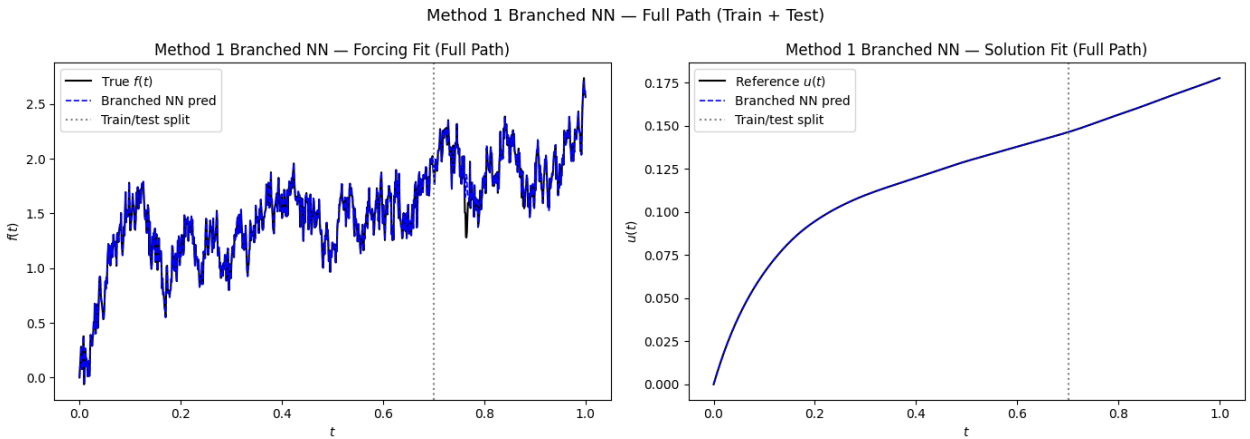


FIGURE 6.6. Forcing and Solution calibration and Prediction for a linear ODE driven by FBM.

6.4. Modeling Nonlinear ODE driven by FBM (Duffing Model). The Duffing oscillator extends the previously mentioned second order SDOF system by adding a nonlinear cubic term. It has a breadth of applications among different fields. [Reynolds et al., 2014] uses the Duffing oscillator to extract information on nonlinear vibrations of timber structures under excitation. In [Mann and Sims, 2009], the authors use a Duffing equation to model an energy harvesting system in

TABLE 5. Relative MSE of the solution u across all variants and methods on the training and testing splits.

	Method 1			Method 2		
	Normal	t -lift	Branched	Normal	t -lift	Branched
Training Solution	6.408e-11	8.301e-11	4.524e-11	2.780e-02	4.597e-02	7.629e-03
Testing Solution	8.600e-11	9.863e-11	1.992e-11	5.811e-02	9.608e-02	1.595e-02

TABLE 6. Relative MSE of the forcing f and solution u for Method 1 (direct forcing match) across all variants on the training and testing splits.

	Training		Testing	
	Forcing	Solution	Forcing	Solution
Normal Solution	2.229e-03	6.408e-11	4.753e-03	8.600e-11
t -lift Solution	2.720e-03	8.301e-11	5.804e-03	9.863e-11
Branched Solution	4.108e-04	4.524e-11	8.766e-04	1.992e-11

TABLE 7. Relative MSE of the integrated forcing target and solution u for Method 2 (integrated target match) across all variants on the training and testing splits.

	Training		Testing	
	Integrated Forcing	Solution	Integrated Forcing	Solution
Normal Solution	6.733e-04	2.780e-02	2.820e+01	5.811e-02
t -lift Solution	1.115e-03	4.597e-02	2.771e+01	9.608e-02
Branched Solution	1.836e-04	7.629e-03	2.863e+01	1.595e-02

response to a magnetic forcing. This concept has also extended to rough signals with gaussian noise within [Green et al., 2012]. A combination of a series derived from the Duffing model and fractional gaussian processes was used to model and simulate asset dynamics within [Yilmaz and Unal, 2019]. The model has been used in complex signal processing with high noise [Deng et al., 2012]. In [Lai and Leng, 2015], Duffing oscillators excited by gaussian noise that produce stochastic resonance are studied in weak signal detection tasks. The model is applied to mechanical engineering tasks such as detecting and diagnosing rolling bearing faults and rotor shaft bending. Likewise, similar problems involving stochastic resonance and noisy signals used within Duffing oscillators for fault detection are presented in [Xiang et al., 2024]. The Duffing oscillator has been extended to be modeled within stochastic frameworks in [Lobo et al., 2019].

We will apply our branched signature kernel method to solve Duffing oscillators of the following standard form with Neumann and Dirichlet boundary conditions as specified in Example 4.5:

Our time values consist of 500 points over the interval 0 to 1. We set $a = 0, b = 1, k_0 = 5, k_1 = 10, \gamma = 10$ as our constants and coefficients. The forcing is taken as a fractional Brownian motion with hurst parameter $H = .4$. The first 70 percent of values are used for training while testing is done on the last 30 percent. We set a signature depth of 2, column robust normalization, and utilize an RBF kernel with $\sigma = 1$. For our solver, we use the approximation method as explained in 4.4. The extension dimension is set at 3.

The results for both the branched model and a baseline model without the branched extension are summarized in table 8. While both models fit extremely well over the entire interval, the branched model showed a 46.5 percent improvement in forcing fit and a 91.3 percent improvement in solution fit overall in comparison to the baseline signature models. This demonstrates the branched model's

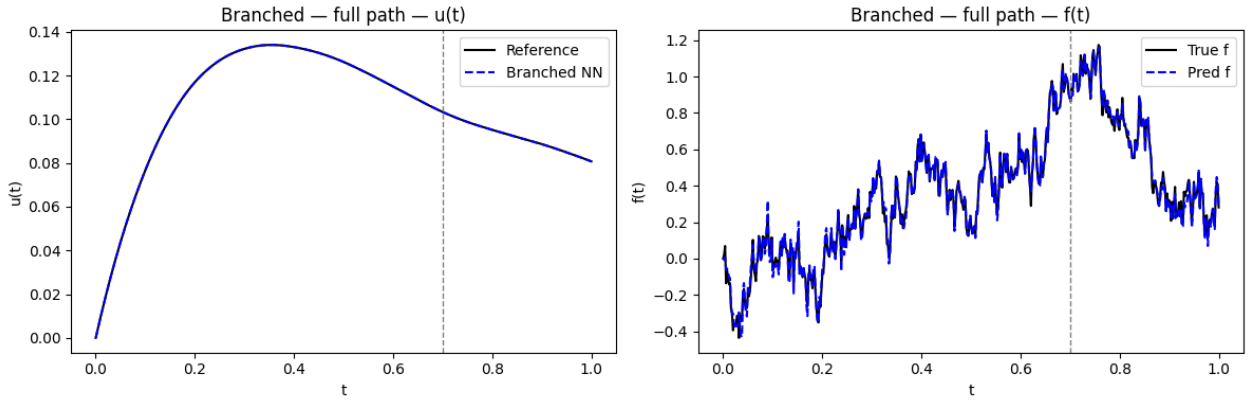


FIGURE 6.7. Branched Signature Kernel Model fit for the Duffing Equation on test- and training interval

ability to encode the branched information not captured by the classical signature. The results for the branched models testing and training fits are presented in figure 6.7

TABLE 8. Relative MSE of the forcing target and solution u for the Duffing model (Method 1) across all variants on the training, testing, and full (train+test) splits.

	Testing		Training		Full	
	Forcing	Solution	Forcing	Solution	Forcing	Solution
Non-branched	1.819e-03	1.862e-08	4.172e-03	1.454e-07	4.172e-03	1.454e-07
Branched	1.101e-03	3.449e-09	2.232e-03	1.258e-08	2.232e-03	1.258e-08

6.5. Variable Coefficient ODE: Arias-Intensity degraded SDOF. We have considered the case of linear ODEs with constant coefficients. However, we may also examine equations in which the coefficients depend on the time or forcing themselves.

Definition 6.1 (Variable Coefficient Second Order Linear ODE).

$$k_1(t, f(t))u''(t) + k_2(t, f(t))u'(t) + k_3(t, f(t))u(t) = f(t), \quad u(0) = a, \quad u'(0) = b,$$

with functions k_1, k_2, k_3 and $x \in [0, T]$.

Previous papers [Li et al., 2000, Li, 1999, Li, 2001] have examined forms of the SDOF system with time-varying coefficients. As long as the coefficient functions themselves do not depend on the solution $u(x)$ or its derivatives, the ODE remains linear in terms of the solution. The signature kernel algorithm does not need to be modified, and only the coefficient function at grid values must be substituted in when solving for the betas and kernel matrix ansatz rather than the constant coefficient. Our solver is therefore easily applicable to modeling ODEs with path-dependent coefficients. Let us once again consider an example from earthquake engineering. The Arias intensity [Arias, 1970]

$$I_A(t) := \frac{\pi}{2g} \int_0^t a(s)^2 ds$$

is a path functional of the ground acceleration that defines earthquake intensity through a measure of the cumulative energy delivered to the structure up to time t . Given a damage source $D(t)$ we may let the effective stiffness decay with response to the damage variable, a well known principle from continuum mechanics [Ramtani, 2013]:

$$k_{eff}(t) = (1 - D(t))k_0.$$

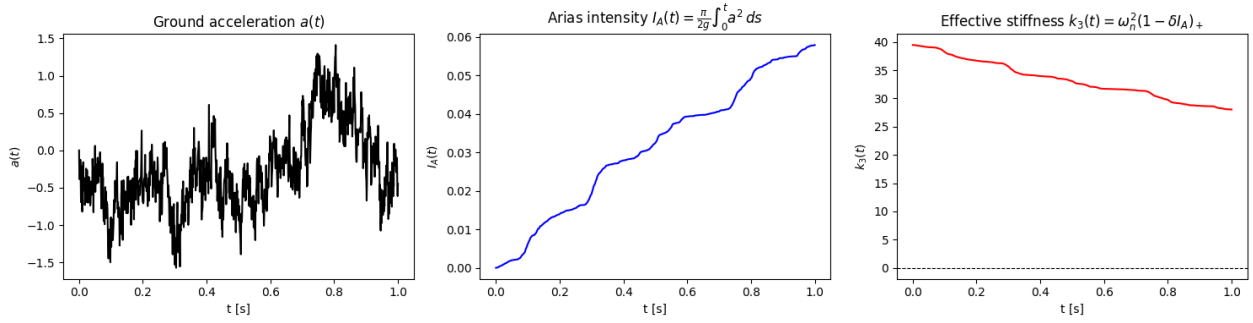


FIGURE 6.8. plots of generated Forcing, Arias Intensity, and Stiffness Coefficient

Dividing by m to be consistent with the third SDOF coefficient:

$$\frac{k_{eff}(t)}{m} = \frac{(1 - D(t))k_0}{m} = (1 - D(t))\omega_0^2.$$

As the Arias intensity strongly correlates with damage and destructive potential [Cabañas et al., 1997], it is plausible to introduce a degradation rate δ and use the intensity as a damage variable, giving us the following variable stiffness coefficient:

$$A_0(t) = \omega_n^2(1 - \delta I_A(t))_+,$$

Where we ensure the stiffness coefficient is non-negative. Inserting into formula 6.1, we arrive at the following model with path-dependent coefficients

Definition 6.2 (Arias-intensity degraded SDOF).

$$\ddot{u}(t) + 2\xi\omega_n\dot{u}(t) + \omega_n^2(1 - \delta I_A(t))_+ u(t) = -9.81 a(t), \quad u(0) = 0, \quad \dot{u}(0) = 0,$$

with degradation rate $\delta \geq 0$ and $(\cdot)_+ := \max(\cdot, 0)$ to guarantee non-negative stiffness. The coefficient $A_0(t) = \omega_n^2(1 - \delta I_A(t))_+$ depends on the forcing path through the cumulative integral $I_A(t)$.

In the collocation framework of (4.5), the blockmatrix becomes

$$L_{ji} = A_2 K_{ji} + A_1 K_{ji}^{(1)} + \omega_n^2(1 - \delta I_A(t_j))_+ K_{ji}^{(2)},$$

with the path-functional value $I_A(t_j) = \frac{\pi}{2g} \sum_{k=0}^{j-1} a(t_k)^2(t_{k+1} - t_k)$ computed once from the count-sampled forcing path $\mathbf{f}_j = (a(t_0), \dots, a(t_j))$. The integral method, streaming protocol, and prediction formulas of Sections 4.3–5 apply unchanged.

We consider an example in which the acceleration $a(t)$ is given by a fractional brownian motion with hurst parameter $H = .2$. We set $\omega_n = 2\pi, \xi = .05, \delta = 5$. 1000 observations are taken over the interval from 0 to 1. Refer to figure 6.8 for plots of the forcing, Arias intensity, and effective stiffness coefficient.

Our signature kernel model uses the neural network lift for the branched extension. The solver uses a signature depth of 2, robust matrix normalization, and utilize an RBF kernel with $\sigma = 1$. We generate 2 extension paths and use approximation method 1 as explained in 4.4. No regression regularization is imposed on the linear solve for beta coefficients. Our signature model is compared to an equivalent approach using a pairwise RBF kernel with the same parameter to illustrate the ability of our model to capture both the path-wise information and the signal roughness. Additionally, we compare to an equivalent signature model, but with no branched extension. The results for the three models in calibration are summarized in table 6.9

As seen in the table, the base RBF Kernel fails to adequately model the forcing, although its solution error is relatively small. The base signature model has much better results, but is unable to capture all of the branched information within the forcing path. The Branched Model shows the best performance out of all models by significant orders of magnitudes. The failure of the RBF in relation to the branched signature model on both the forcing and solution are visualized in figure

TABLE 9. Relative MSE figures for the Arias Intensity Degraded SDOF Problem

Model	Forcing	Solution
RBF (No Signatures) Kernel Model	3.80e-1	2.75e-3
Non-branched Signature Kernel Model	7.68e-5	1.85e-9
Branched Signature Kernel Model	1.80e-7	6.06e-11

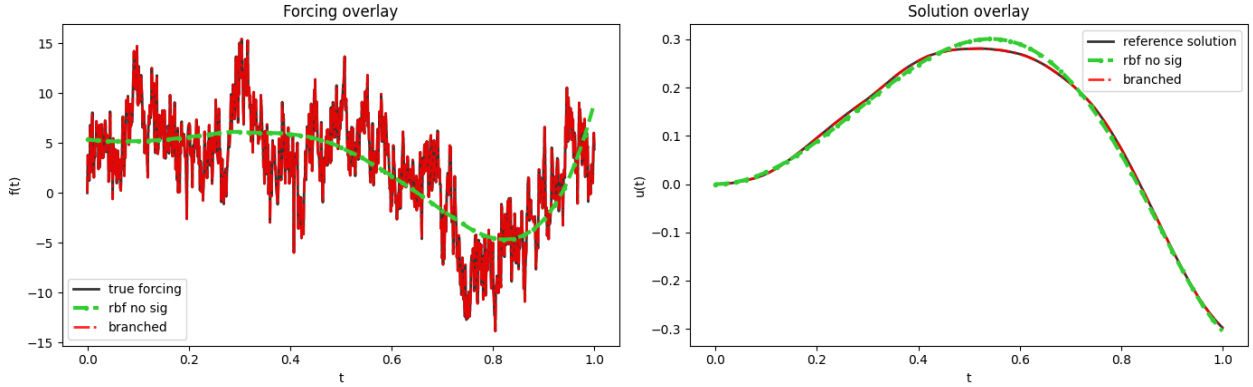


FIGURE 6.9. Calibration results for the branched signature kernel and a point-wise (no signatures) RBF kernel on the Arias Intensity degraded SDOF equation

6.9. The RBF kernel follows the general forcing trend, but does not pick up on the roughness that the branched model does. The solution match is generally accurate for the sole RBF model, but fails to be as accurate as the branched model. We note that the RBF parameter may be "over-tuned", i.e. shrunk extremely small so that the kernel matches the forcings roughness. However, this overfitting leads to a complete inability to predict out of sample. The branched signature kernel model remains able to fit both the forcing and predict out of sample without overfitting to the data. These results demonstrate the superiority of the branched signature kernel model in solving and predicting the solutions of extremely rough differential equations.

6.6. Noisy Kuramoto oscillator system. The general Kuramoto oscillator system [Kuramoto, 1975] on n coupled phase oscillators is given by

$$\frac{d\theta_i}{dt} = \omega_i + \frac{1}{n} \sum_{j=1}^n K_{ij} \sin(\theta_j - \theta_i), \quad i = 1, \dots, n, \quad (6.1)$$

where $\theta_i(t) \in \mathbb{T}$ denotes the phase of the i -th oscillator at time t , $\omega_i \in \mathbb{R}$ is the intrinsic natural frequency, and $K_{ij} \in \mathbb{R}$ denotes the coupling strength between oscillators i and j . Throughout the remainder of this section, n denotes the number of oscillators in the Kuramoto system, distinct from the count-sampled path count N used elsewhere in the paper. If we introduce a standard uniform coupling constant K , and an additive white-noise term ζ_i for each oscillator, we have a new noisy system [Sakaguchi, 1988]

$$\frac{d\theta_i}{dt} = \omega_i + \zeta_i + \frac{K}{n} \sum_{j=1}^n \sin(\theta_j - \theta_i), \quad i = 1, \dots, n. \quad (6.2)$$

The oscillator can equivalently be written in the differential form as follows.

$$d\theta_i(t) = \left[\omega_i + \frac{K}{n} \sum_{j=1}^n \sin(\theta_j - \theta_i) \right] dt + dB_i^H(t), \quad i = 1, \dots, n, \quad (6.3)$$

where $B_i^H(t)$ is a fractional Brownian motion with hurst parameter H . We may write the system (6.2) in the following two equivalent ways:

$$\frac{d\theta_i}{dt} = \omega_i + \frac{K}{n} \sum_{j=1}^n \sin(\theta_j - \theta_i) + \zeta_i(t), \quad \text{or} \quad \frac{d\theta_i}{dt} - \omega_i - \frac{K}{n} \sum_{j=1}^n \sin(\theta_j - \theta_i) = \zeta_i(t).$$

If we wished to study the first form, then one could observe the right hand side of the equation and use the signature kernel algorithm to calibrate the right hand side and recover the solution θ . This can certainly be done as the task is linear and the branched signature captures the variation from the fractional Gaussian noise. We, however, choose to analyze the second form. We will observe the noise and use the nonlinear approximation algorithm to calibrate the left hand side to the right in order to recover the solution by obeying the physical laws.

6.6.1. *Data generation and reference solution.* We first fix a number of oscillators n with frequencies $\omega_i, i = 1, \dots, n$, and a coupling constant K . Then, we choose a uniform grid of N points $0 = t_0, t_1, \dots, t_{N-1} = T$ and set an initial phase vector $\theta(0) = (\theta_1(0), \dots, \theta_n(0))$. For each oscillator i , we then generate a sample path of a fractional Brownian motion $B_i^H(t_0), B_i^H(t_1), \dots, B_i^H(t_{N-1})$ with Hurst parameter H . Using the increments of the fractional Brownian motion, $\Delta B_i^H(t_k) := B_i^H(t_{k+1}) - B_i^H(t_k)$ and time $\Delta t = t_{k+1} - t_k$, for $k = 0, \dots, N-2$, we construct the solution of the system using Euler scheme as follows.

$$\theta_i(t_{k+1}) = \theta_i(t_k) + \left[\omega_i + \frac{K}{n} \sum_{j=1}^n \sin(\theta_j(t_k) - \theta_i(t_k)) \right] \Delta t + \Delta B_i^H(t_k),$$

for $k = 0, \dots, N-2$ and $i = 1, \dots, n$. For signature kernel solver via Method 1 or Method 2 we consider the raw path without any extension to be

$$\mathbf{f}_k = (t_k, \eta_1^H(t_k), \eta_2^H(t_k), \dots, \eta_n^H(t_k)), \quad k = 0, \dots, N-2,$$

where $\eta_i^H(t_k)$ is fractional Gaussian noise and is approximated by

$$\eta_i^H(t_k) \approx \frac{\Delta B_i^H(t_k)}{\Delta t}.$$

6.6.2. *Experiment and results.* For our simulation, we set $n = 3$ oscillators with frequencies of $-1, -3$, and 1.5 respectively. The coupling constant is set to $k = 3$. Each oscillator is driven by a 1000 point fractional Brownian motion with hurst parameter $H = 0.4$. Initial values of θ are selected randomly along the range $[0, 2\pi)$ For our branched model, the signature depth is set to 2, while the extension dimension is set to 3. robust normalization is used along with an RBF kernel with parameter $\sigma = 1$. The branched model is compared to a baseline signature model. Both models used Method 1 applied in its nonlinear form. Results showing fits of the models for the forcing, derivative of the solution, and solution are presented in table 10. Plots of the branched model fits for each oscillators forcing and solution are presented in figure 6.10. Both models are able to fit all oscillators extremely well. However, the branched model shows superior performance in all categories, once again demonstrating its ability to encode information within the branched signature.

TABLE 10. Relative MSE figures for non-branched and branched models for the Noisy Kuramoto Oscillator.

Model	Forcing	$d\theta/dt$	θ
Non-branched Signature Kernel Model	9.00e-6	8.98e-6	5.00e-8
Branched Signature Kernel Model	2.06e-10	5.29e-10	2.47e-8

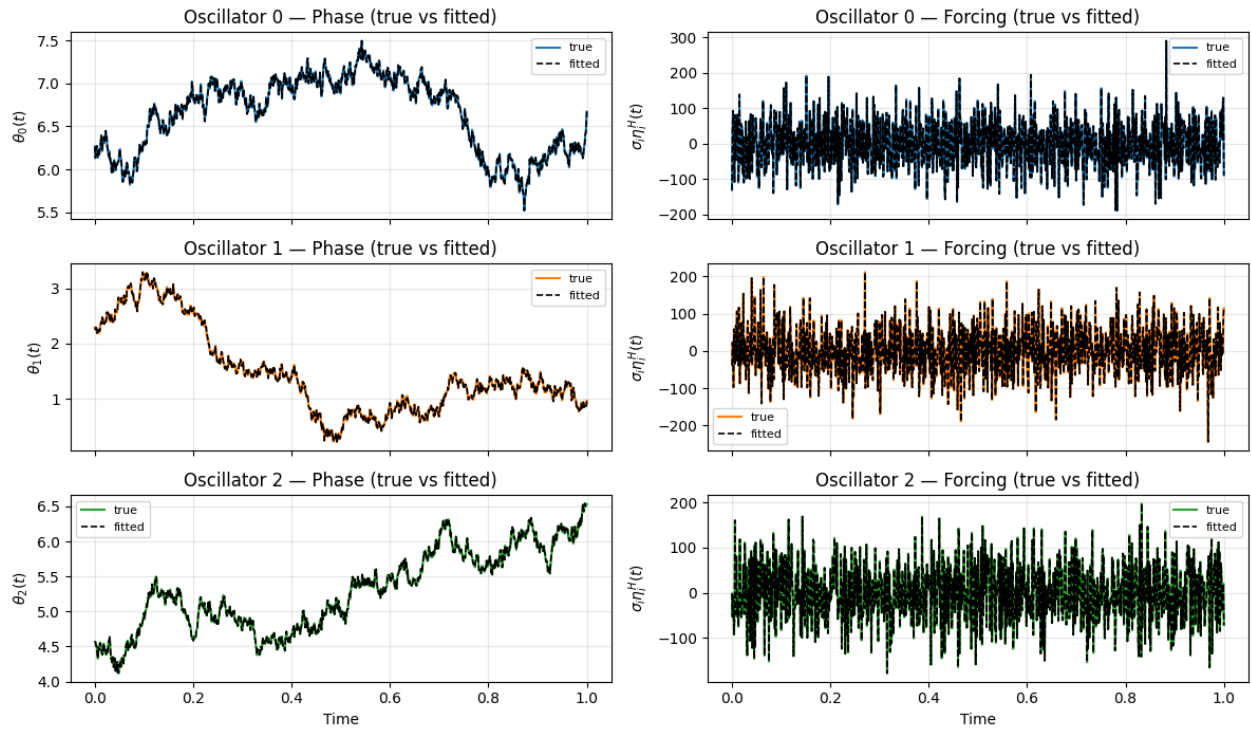
Branched: True vs Fitted $\theta_i(t)$ and $\sigma_i \eta_i^H(t)$ 

FIGURE 6.10. Solution and forcing fits for the branched signature kernel model on the noisy Kuramoto oscillator.

REFERENCES

- [Abbasbandy et al., 2015] Abbasbandy, S., Azarnavid, B., and Alhuthali, M. S. (2015). A shooting reproducing kernel hilbert space method for multiple solutions of nonlinear boundary value problems. *Journal of Computational and Applied Mathematics*, 279:293–305.
- [Ali and Feng, 2025] Ali, M. and Feng, Q. (2025). Branched signature model.
- [Alòs et al., 2025] Alòs, E., Óscar Burés, de Santiago, R., and Vives, J. (2025). Volatility modeling with rough paths: A signature-based alternative to classical expansions.
- [Arias, 1970] Arias, A. (1970). A measure of earthquake intensity. *Seismic Design for Nuclear Power Plants*, R.J. Hansen (ed.), MIT Press, pages 438–483.
- [Bayer et al., 2025] Bayer, C., Gogolashvili, D., and Pelizzari, L. (2025). Local regression on path spaces with signature metrics.
- [Bayraktar et al., 2024] Bayraktar, E., Feng, Q., and Zhang, Z. (2024). Deep signature algorithm for multidimensional path-dependent options. *SIAM Journal on Financial Mathematics*, 15(1):194–214.
- [Boedihardjo et al., 2016] Boedihardjo, H., Geng, X., Lyons, T., and Yang, D. (2016). The signature of a rough path: Uniqueness. *Advances in Mathematics*, 293:720–737.
- [Cabañas et al., 1997] Cabañas, L., Benito, B., and Herráiz, M. (1997). An approach to the measurement of the potential structural damage of earthquake ground motions. *Earthquake Engineering & Structural Dynamics*, 26(1):79–92.
- [Ceylan et al., 2026] Ceylan, M., Kwosek, A. P., and Prömel, D. J. (2026). Universal approximation with signatures of non-geometric rough paths. *arXiv preprint arXiv:2602.05898*.
- [Chen et al., 2021] Chen, Y., Hosseini, B., Owahdi, H., and Stuart, A. M. (2021). Solving and learning nonlinear pdes with gaussian processes.
- [Chevyrev and Kormilitzin, 2025] Chevyrev, I. and Kormilitzin, A. (2025). A primer on the signature method in machine learning. In *Signature Methods in Finance: An Introduction with Computational Applications*, pages 3–64. Springer.
- [Chevyrev and Oberhauser, 2022] Chevyrev, I. and Oberhauser, H. (2022). Signature moments to characterize laws of stochastic processes.

- [Cohen et al., 2023] Cohen, S. N., Lui, S., Malpass, W., Mantoan, G., Nesheim, L., Áureo de Paula, Reeves, A., Scott, C., Small, E., and Yang, L. (2023). Nowcasting with signature methods.
- [Connes and Kreimer, 1999] Connes, A. and Kreimer, D. (1999). Hopf algebras, renormalization and noncommutative geometry. In *Quantum field theory: perspective and prospective*, pages 59–109. Springer.
- [Cox et al., 2026] Cox, S., Khedher, A., and Maessen, T. (2026). Universal approximation by signatures for infinite-dimensional rough paths. *arXiv preprint arXiv:2603.03058*.
- [Cuchiero et al., 2023] Cuchiero, C., Gazzani, G., and Svaluto-Ferro, S. (2023). Signature-based models: theory and calibration. *SIAM journal on financial mathematics*, 14(3):910–957.
- [Cuchiero et al., 2025] Cuchiero, C., Primavera, F., and Svaluto-Ferro, S. (2025). Universal approximation theorems for continuous functions of càdlàg paths and lévy-type signature models. *Finance and Stochastics*, 29(2):289–342.
- [Deng et al., 2012] Deng, X., Liu, H., and Long, T. (2012). A new complex duffing oscillator used in complex signal detection. *Chinese Science Bulletin*, 57.
- [Fang et al., 2023] Fang, B., Ni, H., and Wu, Y. (2023). A neural rde-based model for solving path-dependent pdes.
- [Federal Reserve Bank of St. Louis, 2024] Federal Reserve Bank of St. Louis (2024). Real Gross Domestic Product. <https://fred.stlouisfed.org/series/A191RL1Q225SBEA>. FRED, Federal Reserve Bank of St. Louis. Accessed: 2026-05-19.
- [Feng et al., 2023] Feng, Q., Luo, M., and Zhang, Z. (2023). Deep signature fbsde algorithm.
- [Fornberg and Flyer, 2015] Fornberg, B. and Flyer, N. (2015). Solving pdes with radial basis functions. *Acta Numerica*, 24:215–258.
- [Friz and Victoir, 2010] Friz, P. K. and Victoir, N. B. (2010). *Multidimensional Stochastic Processes as Rough Paths: Theory and Applications*. Cambridge Studies in Advanced Mathematics. Cambridge University Press.
- [Genet and Inzirillo, 2025] Genet, R. and Inzirillo, H. (2025). Keras sig: Efficient path signature computation on gpu in keras 3.
- [Green et al., 2012] Green, P., Worden, K., Atallah, K., and Sims, N. (2012). *The Benefits of Duffing-type Nonlinearities and Electrical Optimisation of a Randomly Excited Energy Harvester*, volume 6, pages 657–667.
- [Gubinelli, 2010] Gubinelli, M. (2010). Ramification of rough paths. *Journal of Differential Equations*, 248(4):693–721.
- [Gyurkó et al., 2013] Gyurkó, L. G., Lyons, T., Kontkowski, M., and Field, J. (2013). Extracting information from the signature of a financial data stream. *arXiv preprint arXiv:1307.7244*.
- [Hairer and Kelly, 2015] Hairer, M. and Kelly, D. (2015). Geometric versus non-geometric rough paths. In *Annales de l’IHP Probabilités et statistiques*, volume 51, pages 207–251.
- [Hambly and Lyons, 2010] Hambly, B. and Lyons, T. (2010). Uniqueness for the signature of a path of bounded variation and the reduced path group. *Annals of Mathematics*, pages 109–167.
- [Hao et al., 2025] Hao, B., Braga-Neto, U., Liu, C., Wang, L., and Zhong, M. (2025). Stability in training pinns for stiff pdes: Why initial conditions matter.
- [Horvath et al., 2023] Horvath, B., Lemercier, M., Liu, C., Lyons, T., and Salvi, C. (2023). Optimal stopping via distribution regression: a higher rank signature approach.
- [Issa et al., 2023] Issa, Z., Horvath, B., Lemercier, M., and Salvi, C. (2023). Non-adversarial training of neural sdes with signature kernel scores.
- [Kansa, 1990a] Kansa, E. (1990a). Multiquadrics – a scattered data approximation scheme with applications to computational fluid-dynamics. ii: Solutions to parabolic, hyperbolic and elliptic partial differential equations. *Computers & Mathematics with Applications*, 19:147–161.
- [Kansa, 1990b] Kansa, E. (1990b). Multiquadrics—a scattered data approximation scheme with applications to computational fluid-dynamics—i surface approximations and partial derivative estimates. *Computers & Mathematics with Applications*, 19(8):127–145.
- [Kidger et al., 2019] Kidger, P., Bonnier, P., Perez Arribas, I., Salvi, C., and Lyons, T. (2019). Deep signature transforms. In *Advances in Neural Information Processing Systems*, volume 32. Curran Associates, Inc.
- [Kidger and Lyons, 2021] Kidger, P. and Lyons, T. (2021). Signatory: differentiable computations of the signature and logsignature transforms, on both CPU and GPU. In *International Conference on Learning Representations*. <https://github.com/patrick-kidger/signatory>.
- [Király and Oberhauser, 2019] Király, F. J. and Oberhauser, H. (2019). Kernels for sequentially ordered data. *Journal of Machine Learning Research*, 20(31):1–45.
- [Krishnapriyan et al., 2021] Krishnapriyan, A., Gholami, A., Zhe, S., Kirby, R., and Mahoney, M. (2021). Characterizing possible failure modes in physics-informed neural networks. In Ranzato, M., Beygelzimer, A., Dauphin, Y., Liang, P., and Vaughan, J. W., editors, *Advances in Neural Information Processing Systems*, volume 34, pages 26548–26560. Curran Associates, Inc.
- [Kuramoto, 1975] Kuramoto, Y. (1975). Self-entrainment of a population of coupled non-linear oscillators. In Araki, H., editor, *International Symposium on Mathematical Problems in Theoretical Physics*, pages 420–422, Berlin, Heidelberg. Springer Berlin Heidelberg.
- [Lai and Leng, 2015] Lai, Z.-H. and Leng, Y.-G. (2015). Generalized parameter-adjusted stochastic resonance of duffing oscillator and its application to weak-signal detection. *Sensors*, 15(9):21327–21349.

- [Lemercier et al., 2021] Lemercier, M., Salvi, C., Damoulas, T., Bonilla, E. V., and Lyons, T. (2021). Distribution regression for sequential data.
- [Levin et al., 2016] Levin, D., Lyons, T., and Ni, H. (2016). Learning from the past, predicting the statistics for the future, learning an evolving system.
- [Li, 2001] Li, Q. (2001). Free vibration of sdof systems with arbitrary time-varying coefficients. *International Journal of Mechanical Sciences*, 43(3):759–770.
- [Li et al., 2000] Li, Q., Fang, J., and Liu, D. (2000). Exact solutions for free vibration of single-degree-of-freedom systems with nonperiodically varying parameters. *Journal of Vibration and Control*, 6:449–462.
- [Li, 1999] Li, Q. S. (1999). A new exact approach for analyzing free vibration of sdof systems with nonperiodically time varying parameters. *Journal of Vibration and Acoustics*, 122(2):175–179.
- [Lobo et al., 2019] Lobo, D., Ritto, T., Castello, D., and Cataldo, E. (2019). Dynamics of a duffing oscillator with the stiffness modeled as a stochastic process. *International Journal of Non-Linear Mechanics*, 116:273–280.
- [Lyons, 2014] Lyons, T. (2014). Rough paths, signatures and the modelling of functions on streams.
- [Lyons and McLeod, 2025] Lyons, T. and McLeod, A. D. (2025). Signature methods in machine learning.
- [Lyons et al., 2020] Lyons, T., Nejad, S., and Perez Arribas, I. (2020). Non-parametric pricing and hedging of exotic derivatives. *Applied Mathematical Finance*, 27(6):457–494.
- [Lyons et al., 2007] Lyons, T. J., Caruana, M., and Lévy, T. (2007). *Differential equations driven by rough paths: Ecole d’Eté de Probabilités de Saint-Flour XXXIV-2004*. Springer.
- [Mann and Sims, 2009] Mann, B. and Sims, N. (2009). Energy harvesting from the nonlinear oscillations of magnetic levitation. *Journal of Sound and Vibration*, 319:515–530.
- [Mohaddes et al., 2025] Mohaddes, A., Iafrate, F., and Lederer, J. (2025). Regularized learning for fractional brownian motion via path signatures.
- [Pannier and Salvi, 2024] Pannier, A. and Salvi, C. (2024). A path-dependent pde solver based on signature kernels.
- [Ramtani, 2013] Ramtani, S. (2013). Basic concepts and models in continuum damage mechanics. Technical report, HAL Open Archive. hal-00776729, <https://hal.science/hal-00776729/document>.
- [Reizenstein and Graham, 2020] Reizenstein, J. and Graham, B. (2020). Algorithm 1004: The iisignature library: Efficient calculation of iterated-integral signatures and log signatures. *ACM Transactions on Mathematical Software (TOMS)*.
- [Reynolds et al., 2014] Reynolds, T., Harris, R., and Chang, W.-S. (2014). Nonlinear pre-yield modal properties of timber structures with large-diameter steel dowel connections. *Engineering Structures*, 76:235–244.
- [Sabate-Vidales et al., 2020] Sabate-Vidales, M., Šiška, D., and Szpruch, L. (2020). Solving path dependent pdes with lstm networks and path signatures.
- [Sakaguchi, 1988] Sakaguchi, H. (1988). Cooperative phenomena in coupled oscillator systems under external fields. *Progress of theoretical physics*, 79(1):39–46.
- [Salvi et al., 2021] Salvi, C., Cass, T., Foster, J., Lyons, T., and Yang, W. (2021). The signature kernel is the solution of a goursat pde. *SIAM Journal on Mathematics of Data Science*, 3(3):873–899.
- [Shmelev and Salvi, 2025] Shmelev, D. and Salvi, C. (2025). pysiglib – fast signature-based computations on cpu and gpu.
- [Solow, 1956] Solow, R. M. (1956). A contribution to the theory of economic growth. *The Quarterly Journal of Economics*, 70(1):65–94.
- [Tóth et al., 2025] Tóth, C., Cruz, D. J. D., and Oberhauser, H. (2025). A user’s guide to KSig: Gpu-accelerated computation of the signature kernel. *arXiv preprint arXiv:2501.07145*.
- [Toth et al., 2024] Toth, C., Oberhauser, H., and Szabo, Z. (2024). Random fourier signature features.
- [Vibrationdata,] Vibrationdata. El centro earthquake.
- [Wang et al., 2024] Wang, S., Sankaran, S., and Perdikaris, P. (2024). Respecting causality for training physics-informed neural networks. *Computer Methods in Applied Mechanics and Engineering*, 421:116813.
- [Wang et al., 2021] Wang, S., Teng, Y., and Perdikaris, P. (2021). Understanding and mitigating gradient flow pathologies in physics-informed neural networks. *SIAM Journal on Scientific Computing*, 43(5):A3055–A3081.
- [Xiang et al., 2024] Xiang, J., Guo, J., and Li, X. (2024). A two-stage duffing equation-based oscillator and stochastic resonance for mechanical fault diagnosis. *Chaos, Solitons & Fractals*, 182:114755.
- [Yilmaz and Unal, 2019] Yilmaz, A. and Unal, G. (2019). Stochastic duffing equation in modelling of financial time series. *International Journal of Dynamics and Control*, 7:1–22.
- [Zeng and Jiang, 2025] Zeng, P. and Jiang, S. (2025). Semi-parametric functional classification via path signatures logistic regression.